

DISCRETE AND CONTINUUM RELAXATION DYNAMICS OF FACETED CRYSTAL SURFACE IN EVAPORATION MODEL

KANNA NAKAMURA* AND DIONISIOS MARGETIS†

Abstract. We study the connection of two scales in the relaxation of axisymmetric crystal surfaces with a facet via an ad hoc evaporation-condensation model. We provide numerical evidence that the continuum slope determined under “natural boundary conditions” at the facet, which are derived solely from continuum thermodynamics, follows closely the underlying discrete dynamics. At the microscale, the discrete scheme consists of a large system of differential equations for the radii of repulsively interacting line defects (steps) separated by terraces. We solve this system numerically and thereby describe step collapses on top of the facet. Each step velocity is proportional to the step chemical potential, the variation of the total step free energy; the relevant discrete mobility is assumed linear in the width of the upper terrace. At the macroscale, the facet is a free boundary for a second-order, diffusion-like, nonlinear partial differential equation for the slope, which we study via the extended gradient method, boundary layer theory and a self-similarity ansatz. The proof of convergence of the discrete (step) scheme to the continuum solution is not addressed.

Key words. crystal surface, evaporation, facet, Burton-Cabrera-Frank (BCF) model, subgradient formulation, boundary layer

AMS subject classifications. 74A50, 35Q99, 35R35

1. Introduction. A challenging issue in non-equilibrium statistical mechanics is to connect the dynamics of large particle systems to macroscopic evolution laws amenable to computation and physically motivated predictions. Traditionally, much insight into the kinetic limits of interacting particles has been gained in the context of gas theory and the Boltzmann equation; see e.g. [5,58]. Inspired by these developments and recent experimental advances, research efforts seek to analyze macroscopic limits of other physical systems, particularly crystalline solids evolving near equilibrium.

The evolution of material surfaces and interfaces near equilibrium is often subject to variational principles. In particular, crystal surfaces and grain boundaries relax, in the absence of external material deposition, so that the flow of height profiles stems from the variation of thermodynamics-based free energies (see, e.g. [7, 21, 23, 27, 33, 36, 44, 51, 59, 60]).

Below the roughening transition temperature, the crystal surface morphological evolution is caused by the motion of atomic line defects (steps), which can be viewed as particles, and can be characterized by macroscopic plateaus called *facets* [6, 8, 32, 42, 43, 50]. At the *microscale*, the equations of motion are large systems of differential equations for step positions [17, 30, 31]. At the *macroscale*, away from facets, the surface is described by partial differential equations (PDEs) for the surface height or slope [14, 46, 48, 52, 59], which are more amenable to analytical predictions. The connection of the two scales across surface peaks, valleys and facets is not adequately understood.

*Department of Mathematics, University of Maryland, College Park, MD 20742-4015 (nakamura@math.umd.edu). This author’s research was supported by a Graduate Student Summer Research Fellowship during the summer of 2011 and by NSF DMS-0847587 at the University of Maryland.

†Department of Mathematics, and Institute for Physical Science and Technology, and Center for Scientific Computation and Mathematical Modeling, University of Maryland, College Park, MD 20742-4015 (dio@math.umd.edu). This author’s research was supported by NSF DMS-0847587 at the University of Maryland.

In this article, we aim to show that two distinct approaches, each based on the above respective description, can be *reconciled* within a certain ad hoc (yet physically motivated) evaporation model in the absence of external material deposition from above and nucleation. One of these approaches follows the motion of steps; and has indicated that individual steps on top of facets can influence surface profiles macroscopically [10, 30, 31, 39, 55]. Another approach relies on PDEs outside facets with boundary conditions applied at the moving (“free”) facet boundaries via continuum thermodynamics [38, 59]. This latter view is appealing since it is subject to a variational formulation [33, 56]; however, for surface diffusion this approach is known to produce results that are in principle *not* consistent with step motion [30, 31, 39]. Here, we provide a, previously unnoticed, paradigm of step kinetics in which the two approaches are mutually consistent across the facet of an axisymmetric structure.

Our intention is to shed light on the issue of how continuum thermodynamics is related to underlying discrete schemes when step collapses occur on top of facets. Evidently, the number of steps is not conserved in our radial setting. It is tempting to expect that this property implies lack of consistency of the discrete system with the thermodynamics-based continuum limit [30, 31]. Most, but by no means all [34], previous studies of facet evolution focus on surface diffusion in the absence of evaporation; see, e.g., [1, 2, 30, 31, 39]. In [34], the authors point out the significant influence of kinetics, especially nucleation, on the connection of continuum laws (i.e., the Hamilton-Jacobi equation for the height) to step motion near facets.

Here, we study aspects of evaporation dynamics. Evaporation, in which adsorbed atoms (adatoms) are exchanged between steps and the surrounding vapor, is ubiquitous in epitaxial phenomena [26, 50]. In principle, evaporation coexists with, but is simpler to study than, surface diffusion. In the latter process, adatoms diffuse on terraces and on step edges, and attach or detach at steps from or to terraces [32, 50].

To capture with minimal complexity the main elements that may cause close agreement of discrete and continuum-scale dynamics, we focus on an ad hoc yet physically plausible evaporation model that is rich enough to include step curvature, elastic-dipole step-step repulsions [37, 45], and a terrace-width-dependent discrete step mobility. We are not aware if this simplified model has a concrete physical application.¹ Nonetheless, we anticipate that the model can serve as a reference case in the study of realistic, more complicated microscopic theories. In fact, we also discuss how our model results from the simplification of a step scheme that includes desorption, surface diffusion, and a negative (“inverse”) Ehrlich-Schwoebel (ES) effect [15, 49, 53, 54, 57], by which adatoms on terraces attach/detach at down-steps with a kinetic rate that is larger than the rate for up-steps.

At the macroscale, our model reduces to a description of generic appeal: The flow of the continuum-scale height is expressed as the variation of a familiar singular surface free energy, which we consider as given [24, 59]. At the level of steps, the step velocity is proportional to the step chemical potential, the variation of a total step free energy, which we also consider as given; the respective coefficient, or discrete mobility, is chosen linear in the width of the *upper* terrace, giving rise to a forward difference scheme and stable step dynamics in the radial setting.

Our work has limitations. For instance, our analysis of the continuum limit is formal. We only provide numerical evidence that a solution of the discrete scheme for our ad hoc model approaches a solution of the thermodynamics-based continuum limit. A rigorous proof of this convergence is presently elusive. The step model

¹Hence, we consider our assumed discrete dynamics as a toy model.

can of course be enriched to include more realistic physical effects such as non-radial geometries but this task is left for future work.

We assume that the reader is familiar with the fundamentals of epitaxial growth. For broad reviews on the subject, see, e.g. [32, 42, 43].

1.1. Microscopic model. Two of our reasons for choosing the particular evaporation model are: (i) its compatibility with the known thermodynamics-based PDE outside facets [33, 59]; and (ii) the well-posedness of the ensuing discrete dynamics problem even for *zero* step-step interaction. Our results aim to illustrate the intimate connection of a special discrete model (and the underlying kinetics) to a well-studied continuum description. Below, we outline how our ad hoc model can be viewed as a variant of a certain model of surface diffusion on stepped surfaces.

1.1.1. Motivation. In our toy model, the step velocity law is

$$(1.1) \quad dr_i/dt = \dot{r}_i = -\nu_i(\mu_i - \mu^0),$$

which expresses an exchange of adatoms between concentric circular step edges and the surrounding vapor. In (1.1), $r_i(t)$ is the i th step radius, ν_i is the step mobility (specified below), μ^0 is the constant chemical potential of the surrounding vapor, and μ_i is the step chemical potential; this μ_i incorporates two effects, namely, step curvature (stiffness) and step-step elastic-dipole interactions [32]. We then obtain a large system of coupled nonlinear ordinary differential equations (ODEs) for the step radii. This system is expected to describe successive annihilations of the top (extremal) layers of an axisymmetric structure. Of course, the height of the surface structure is expected to decrease with time. Here, we use $\nu_i \propto r_i - r_{i-1} > 0$ and $\mu^0 = 0$ in (1.1); the corresponding model is referred to as M1, the focus of this article.

The formulation of M1 can be partly motivated with recourse to successive simplifications of a discrete scheme based on surface diffusion and desorption (see section 6.2). The starting model, herein called M3, is derived directly from the Burton-Cabrera-Frank (BCF) theory of step flow [8]. The step velocity law for M3 is

$$(1.2) \quad \dot{r}_i = -\nu \mathcal{G} (r_i - r_{i-1})(\mathcal{T} + \mu_i), \quad \mathcal{G} = \frac{r_i + r_{i-1}}{2r_i},$$

where ν is a constant and \mathcal{T} is the Boltzmann energy (absolute temperature in units where $k_B = 1$). Note that in (1.2) the associated coefficient of μ_i (step mobility) is different from that in M1 due to the appearance of the geometric factor \mathcal{G} which substantially influences the velocity of the top step. Away from the facet, (1.2) gives rise to a formal continuum limit for the *slope* profile same as M1. The discrete equations of motion for M3 stem from a special limit of three combined kinetic processes [50]: (i) atom evaporation (with finite desorption time, τ); (ii) adatom terrace diffusion; and (iii) inverse ES effect. The procedure for obtaining (1.2) is outlined in section 6.2.

The model M3 can be further simplified by removal of (the constant) \mathcal{T} from (1.2). Thus, we wind up with the modified step velocity law

$$(1.3) \quad \dot{r}_i = -\nu \mathcal{G} (r_i - r_{i-1})\mu_i.$$

The model corresponding to (1.3) will be henceforth called M2. Our numerical simulations (section 6.2) indicate that, at long time and many steps, M2 admits self-similar solutions for the discrete slopes, $M_i \propto (r_i - r_{i-1})^{-1}$, with similarity variable $\xi_i = r_i/\sqrt{t}$.²

²On the other hand, ODEs (1.2) of M3 are not expected to allow for a self-similar behavior. This aspect is not studied any further here.

The last stage of our simplifications leading to M1 is to replace \mathcal{G} by 1 in (1.3). Strictly speaking, this approximation is valid when $r_i - r_{i-1} \ll r_i$ but is expected to break down near the top step (where $r_i - r_{i-1} \approx r_i$). This approximation is close to the spirit of the continuum limit.

Interestingly, we demonstrate numerically that the discrete slopes produced by M1 are in excellent agreement with the continuum slope of the thermodynamics-based approach. By contrast, discrete slopes by M2 are *not* compatible with the thermodynamics-based continuum theory. This observation exemplifies the role of extremal steps in facet evolution. Models M2 and M3 are the subjects of future work.

1.1.2. Properties of M1. One of our goals is to understand the behavior of steps moving according to model M1. For this purpose, we first prove the existence of a unique solution to ODE system (1.1), with the mobility $\nu_i \propto r_i - r_{i-1}$. Along with this proof, we show that, in contrast to the surface diffusion case [17], the discrete dynamics (forward scheme) here do *not* allow for step collisions even in the absence of step interactions; hence, the ordering of steps, i.e., the property $r_i(t) > r_{i-1}(t)$, is preserved by the flow and steps do not touch provided $r_i(0) > r_{i-1}(0)$ for all i .

Furthermore, we solve numerically ODEs (1.1) for many steps and thereby compute the discrete slopes $M_i = a/(r_i - r_{i-1})$, where a is a step height, for all times $t \geq 0$. Our numerical data provides evidence that, for large enough t , the times t_n at which the top steps are annihilated behave as $t_n \approx cn^\beta$ for $n \gg 1$; n enumerates steps in the initial configuration and the constants c and β depend on the material parameters and the initial data [17,30]. To simplify the numerics, we assume an initial conical profile, for which we find $\beta = 2$. In addition, we numerically observe that, consistent with the above behavior of t_n , the discrete slopes, M_i , exhibit a self-similar behavior, which is not uncommon for the radial geometry [30,35,61,62].

The case with non-interacting steps deserves some special attention. By computing exactly the radii of the top two steps explicitly as functions of time, we are able to test the validity of our numerics in this special case.

1.2. Macroscopic limit and facet problem. In the limit of a large number of steps, the ODE system for steps is expected to reduce to evolution PDEs for the surface height and slope profiles away from the facet; in our setting, the facet is a region of spatially constant height. The rigorous study of this continuum limit lies beyond our scope. In our formal discussion of this limit we primarily invoke the (relatively simple) notion of pointwise convergence in order to express the passage from the ODEs to the PDEs; this choice circumvents subtleties of weak convergence, which may be a more appropriate notion for our system. The main assumption for the validity of the continuum limit is that the terrace width is much smaller than the radii of its bounding steps and varies slowly with the spatial (polar) coordinate.³

Within the continuum framework, there are at least two treatments of the facet. One treatment is to apply the PDE (outside the facet) and view the facet edge as a free boundary via enforcing appropriate boundary conditions [59]. Another treatment is to extend the continuum theory *everywhere*, including the facet, by replacing the PDE by a variational statement according to the known subgradient (extended gradient) formulation [33]. The two treatments can of course become mutually consistent if the facet boundary conditions are chosen to be the “natural boundary conditions” coming from the variational formulation; these conditions are the continuity of height, of a

³In a rigorous analysis, this last assertion should not be an assumption but instead be deduced from the discrete dynamics. We do not address the related issues here.

radial vector interpreted as the flux germane to the height change with time, and of slope for interacting steps (see section 5.1). We mainly choose these conditions in this article; hence, we essentially make no distinction between the subgradient and the free boundary approaches here (see, however, the discussion of section 5.1.2).

In our evaporation-condensation model M1, the large-scale slope profile predicted via the subgradient formulation is found by numerics to be fully consistent with the collapses of steps near the expanding facet. Our result implies that, in this particular system, no information on the near-facet behavior is left out by the direct coarse-graining of the discrete dynamics outside the facet.

We study the PDE for the slope profile (outside the facet) numerically, and analytically via natural boundary conditions at the facet boundary [33, 59]. In the non-interacting case, the PDE solution is determined exactly; it has a self-similar structure and suggests treating the facet as a shock-like wave [19]. We extend the shock wave notion to interacting steps. In this case, we solve the PDE numerically via self-similarity of the slope, and gain some understanding of the (classical) solution via boundary layer theory near the facet for weak step interactions, in the spirit of [38].

A note on previous works is in order. Progress in understanding the connection of step flow and continuum theory has been made for semi-infinite facets at *fixed* heights in one space dimension (1D) [1, 2, 41]. In this case, the surface height is a convenient independent variable, by which the need to use a free boundary for the facet is circumvented; furthermore, step collapses do not occur and, thus, the total number of steps is preserved. The analysis becomes more involved for periodic surface corrugations in 1D [31, 47] and radial geometries [30, 39] which have *variable* facet heights. For such geometries, boundary conditions consistent with step flow should in principle invoke microscopic parameters, e.g., step collapse times, which non-trivially result from solving the discrete schemes for steps [30, 39].

1.3. Limitations. A couple of limitations of our study should be spelled out. A rigorous proof for the convergence of the step ODE solution for M1 to the continuum thermodynamics-based solution is not addressed here. We believe that a convenient starting point for the analysis would be to formulate, by using appropriate variables, the step ODEs as the steepest descent of a convex energy (see, e.g. [1, 2]). This would indicate a treatment analogous to approaches in numerical (convex) analysis. Some relevant analysis using the finite element method has been carried out in recent years [3, 11]. We note that, by contrast to a numerical analysis approach in which one starts from a given PDE and has the freedom to choose a convenient discretization scheme, here one is bound to the given discrete step structure, e.g. the form of the step chemical potential. Exploring the connection of our model to methods of numerical analysis or dynamical systems is the subject of work in progress.

Other possible developments of our study include investigating richer kinetics (e.g., material deposition from above or nucleation) [50]. Furthermore, we only study conical initial profiles; extension of our work to other initial geometries in two space dimensions (2D) is unexplored. Another limitation concerns our observation of self-similar slope profiles: we currently lack a rigorous understanding of this apparent behavior even in the radial setting.

1.4. Outline. The remainder of the paper is organized as follows. In section 2, we describe the geometry and discrete equations of motion. In section 3, we give a proof for the existence of a unique solution to the ODE system of M1; we also prove the corresponding non-crossing property for steps. In section 4, we review the formal continuum limit for the height and slope profiles away from the facet. In section 5, we

compute thermodynamics-based PDE solutions and compare them to discrete (step) simulations. In section 6, we discuss a shock wave interpretation of the continuum solution; and a connection of our discrete model M1 with M3 and M2 on the basis of the BCF theory. In section 7, we summarize our results and outline a few open problems. The appendices provide technical derivations invoked in the main text.

1.5. Notation conventions. The relation $f = \mathcal{O}(g)$ implies that f/g is bounded as a variable approaches a limit; similarly, $f \sim g$ means that $(f-g)/f$ approaches zero when a variable tends to a given limit. A dot on top of a symbol denotes derivative with respect to time, e.g., $\dot{r} = dr/dt$. The symbols \mathbb{N} and $(x_i)_{i \in I}$ denote the set of natural numbers and a vector indexed by the set I , respectively; and $B^d(\mathbf{r}, \delta)$ is the open ball of radius $\delta > 0$ centered at point \mathbf{r} in d space dimensions (Euclidean space \mathbb{R}^d), where boldface symbols denote vectors in the main text (but not in Appendix A).

2. Formulation.

2.1. Geometry. The geometry is shown in Figure 2.1. At the macroscale, the crystal surface is described by a continuous height profile, $h(r, t)$, with respect to a fixed (xy -) plane of reference, where r is the polar coordinate and t is time ($r \geq 0$, $t \geq 0$). The (circular) facet has zero slope orientation, height $h_f(t)$ and radius $r_f(t)$. We expect that $\dot{r}_f(t) \geq 0$, i.e., the facet expands, by analogy with the surface diffusion case [38].

At the microscale, this configuration consists of concentric circular layers (steps) of constant atomic height, a . The i th step has radius $r_i(t)$, where initially (at time $t = 0$) $i = 0, 1, \dots, N$ and $N \gg 1$; by convention, $r_{-1} \equiv 0$ (cf. (2.4)). We take N to be large yet finite, so that the structure can be considered as semi-infinite for all practical purposes (but not in section 3.2). Steps are expected to shrink and collapse on top of the facet; only steps with $n \leq i \leq N$ are present at times $t_{n-1} \leq t < t_n$, where t_n is the collapse time of the n th step of the initial configuration; by convention, set $r_{n-1}(t) \equiv 0$ if $t \geq t_{n-1}$ ($n \geq 0$) where $t_{-1} = 0$. Thus, i is a variable index enumerating steps that remain on the structure relative to the initial configuration.

We assume that $r_{i+1}(0) > r_i(0)$ for all i .⁴ Then, the discrete slopes defined by

$$(2.1) \quad M_i = \frac{a}{r_{i+1} - r_i}$$

are positive ($M_i > 0$) and bounded, $M_i \leq \mathcal{O}(1)$. Near the top step, $r_{i+1} - r_i$ is much larger than a ; thus, M_i is small (as we will show numerically).

Let $h_{\text{top}}(t)$ denote the height of the top layer at time t (see Figure 2.1). Because of step collapses on top of the facet, $h_{\text{top}}(t)$ must decay; evidently, $0 < h_{\text{top}} - h_f = \mathcal{O}(a) \downarrow 0$ in the macroscopic limit. The everywhere-continuous surface height, $h(r, t)$, is the continuum limit of the discrete (piecewise constant) height $h_d(r, t)$ which satisfies

$$(2.2) \quad h_{\text{top}}(t) - h_d(r, t) = (i - n)a,$$

for $r_{i-1} < r < r_i$ and $t_{n-1} \leq t < t_n$. In the continuum limit, where $a \rightarrow 0$ and $ia = \mathcal{O}(1)$, we can assert that

$$(2.3) \quad ia \rightarrow h_f(0) - h(r, t).$$

⁴If $r_{i+1}(0) > r_i(0)$ (initially), the relation $r_{i+1}(t) > r_i(t)$ for all later times, $t > 0$, should follow from the step flow equations. We provide a proof of this property in section 3.

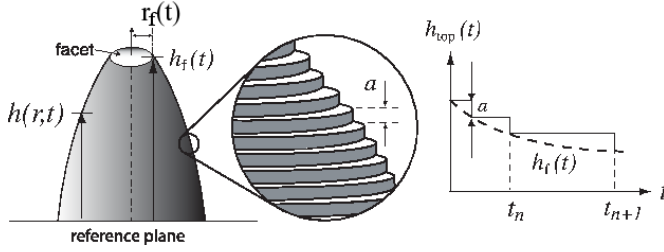


FIG. 2.1. Schematic of axisymmetric surface structure with a facet. At the macroscale, the height, $h(r,t)$, is continuous; the facet height and radius are $h_f(t)$ and $r_f(t)$. At the microscale, circular steps of atomic size a are evident and the height is uniformly discretized; t_n is the n -th step collapse time where n enumerates steps in the initial configuration.

2.2. Discrete equations of motion. Next, we formulate the discrete equations of motion for an evaporation-condensation model. The (radial) velocity of the i th step stems from (1.1) and is assumed to be

$$(2.4) \quad \dot{r}_i = -\nu \frac{r_i - r_{i-1}}{a} (\mu_i - \mu^0),$$

for all i of interest ($n \leq i \leq N$), where ν is a constant that has units of length/energy/time; recall that $r_{i-1}(t) \equiv 0$ if $i \leq n$, $t_{n-1} \leq t < t_n$. In the limit $a \rightarrow 0$, (2.4) becomes $\partial_t h = -\nu \mu$, where μ is the macroscopic limit of μ_i , in agreement with a continuum-scale model in [59] (see section 4 for details). Note that velocity law (2.4) updates each step position through values for smaller step index, i ; thus, we consider (2.4) as a forward discrete scheme (in i).

To determine μ_i , we first describe the total step free energy, E^{st} , which accounts for step line tension as well as entropic and elastic-dipole step repulsive interactions:

$$(2.5) \quad E^{\text{st}}(t; a) = \sum_{i=n}^N 2\pi r_i(t) [g_1 a + \mathcal{V}(r_i(t), r_{i+1}(t); a)],$$

where the pairwise interaction energy between steps of radii r and ρ is [30, 38, 40]

$$(2.6) \quad 2\pi r \mathcal{V}(r, \rho; a) = 2\pi \check{g}_3 \frac{r\rho}{\rho + r} \left(\frac{a}{\rho - r} \right)^2.$$

In (2.5) and (2.6), $g_1 a$ is the step line tension (energy/length) and \check{g}_3 expresses the strength of step-step repulsion per unit length of a step [38]; for later algebraic convenience in comparing discrete and continuum slopes, we replace \check{g}_3 by the (macroscopic) parameter [38]

$$(2.7) \quad g_3 = \frac{3}{2} \frac{\check{g}_3}{a}.$$

The step chemical potential is defined through the variational formula [40]

$$(2.8) \quad \sum_i a \oint_{L_i} \mu_i v_i ds = \Omega \dot{E}^{\text{st}}(t; a),$$

where L_i is the i -th step curve and v_i is the step velocity. Relation (2.8) implies

$$\begin{aligned}
\mu_i &= \frac{\Omega}{a} \frac{1}{2\pi r_i} \frac{\partial E^{\text{st}}}{\partial r_i} \\
&= \frac{\Omega g_1}{r_i} + \frac{\Omega}{r_i a} \frac{\partial \{r_i [\mathcal{V}(r_i, r_{i+1}) + \mathcal{V}(r_{i-1}, r_i)]\}}{\partial r_i} \\
(2.9) \quad &= \frac{\Omega g_1}{r_i} + \frac{2}{3} \Omega \frac{g_3 a^2}{r_i} \left\{ \psi(r_i, r_{i+1}) - \psi(r_{i-1}, r_i) + \frac{1}{r_i^2} [\phi(r_i, r_{i+1}) + \phi(r_{i-1}, r_i)] \right\},
\end{aligned}$$

where Ω is the atomic volume, $\Omega \approx a^3$, and

$$(2.10) \quad \psi(r, \rho) = \frac{2r\rho}{\rho + r} \frac{1}{(\rho - r)^3},$$

$$(2.11) \quad \phi(r, \rho) = \left(\frac{\rho r}{\rho + r} \right)^2 \frac{1}{(\rho - r)^2}.$$

Accordingly, we obtain the step velocity law

$$\begin{aligned}
\dot{r}_i &= -\frac{\Omega \nu g_1}{r_i} \frac{r_i - r_{i-1}}{a} \left\{ 1 + \frac{2g_3 a^2}{3} \left[\psi(r_i, r_{i+1}) \right. \right. \\
(2.12) \quad &\quad \left. \left. - \psi(r_{i-1}, r_i) + \frac{\phi(r_i, r_{i+1}) + \phi(r_{i-1}, r_i)}{r_i^2} \right] \right\},
\end{aligned}$$

where $n \leq i \leq N$ for $t_{n-1} < t < t_n$ and $r_{N+1}(t) \equiv 0$. The parameter $g \equiv g_3/g_1$ expresses the relative strength of step line tension and step-step repulsion.

REMARK 2.1. Equation (2.12) can be non-dimensionalized by use of the variables $\tilde{r}_i = r_i/a$ and $\tilde{t} = (\nu g_1 \Omega/a^2)t$; or, alternatively, via units with $a = 1 = \nu g_1$. We follow this route in sections 3 and 5.2–5.4. In sections 4 and 6, we choose to use dimensional variables so as to indicate more transparently the passage to and nature of the continuum limit outside the facet.

3. Existence of unique solution. In this section, we prove that, in some contrast to diffusion-limited kinetics [17], steps do *not* collide in our model even for zero step interactions. We give separate proofs for $g = 0$ and $g \neq 0$. For $g = 0$, our proof is uniform in the initial step number, N , whereas the uniformity is lost in the case with nonzero g . Thus, for $g = 0$ we can strictly consider a semi-infinite surface structure. Note that our choice of (radial) geometry is perhaps the simplest one for which step motion is rich enough even for vanishing interaction; in 1D, the $g = 0$ case is trivial.

3.1. Case with $g=0$. The absence of step collisions can be loosely explained by inspection of (2.12) for $g = 0$. Suppose two steps tend to coalesce at some time; then, the innermost step moves faster whereas the other step is slowed down (because of the governing forward scheme), and step collision is thus avoided. Note that the assumed forward scheme is deemed natural in our setting, given that the preferred direction of motion of each step (with a minus sign in (2.4)) is *towards* the origin.

The main result of this subsection can be stated as follows.

THEOREM 3.1. *Let $N \in \mathbb{N}$ be the initial number of steps and $I = \{0, 1, \dots, N\}$. Consider the vectors $\mathbf{r}(t) = (r_0(t), r_1(t), \dots, r_N(t))$ and $\mathbf{f}(\mathbf{r}) = (f_0(\mathbf{r}), f_1(\mathbf{r}), \dots, f_N(\mathbf{r}))$ where*

$$(3.1) \quad f_i(\mathbf{r}) = \begin{cases} -\frac{r_i - r_{i-1}}{r_i} & r_i \neq 0 \\ 0 & r_i = 0 \end{cases},$$

and $r_{-1}(t) \equiv 0$ in the definition of f_0 .

Then, there exists a unique global solution to the initial value problem (IVP)

$$(3.2) \quad \dot{\mathbf{r}} = \mathbf{f}(\mathbf{r}), \quad \mathbf{r}(0) = \mathbf{r}^{in}, \quad \mathbf{r}^{in} \in W = \{\mathbf{x} \in \mathbb{R}^N \mid 0 < x_0 < \dots < x_N\}$$

in the domain $\Omega = \{\mathbf{x} = (x_i)_{i \in I} \mid x_i \neq 0, i \in I\}$. Furthermore, this solution stays in W for $t \in [0, t_0)$ and in $W_i = \{\mathbf{x} \in \mathbb{R}^N \mid 0 = x_0 = \dots = x_i, x_{i+1} < \dots < x_N\}$ for $t \in [t_i, t_{i+1})$, where t_i is the time when r_i reaches 0; here, $0 < t_0 < t_1 < \dots < t_N < \infty$. The solution is smooth for all $t \neq t_0, \dots, t_N$. More precisely, $r_i(t)$ is continuous for all t and smooth on $[0, t_i)$.

Proof. First, we prove the existence of a unique local solution to problem (3.2). Observe that each f_i is smooth on W with $\nabla f_i = (0, \dots, 0, \frac{1}{r_i}, -\frac{r_{i-1}}{r_i^2}, 0, \dots, 0)$. So, for every $\mathbf{r} \in W$, let $0 < \delta < \min_{i \in I} \{r_i\}$. Then, for any $\mathbf{y} \in B^N(\mathbf{r}, \delta)$ we have

$$(3.3) \quad |\nabla f_i(\mathbf{y})|^2 = \frac{1}{y_i^2} + \frac{y_{i-1}^2}{y_i^4} \leq \left(\frac{1}{r_i - \delta}\right)^2 + \frac{(r_{i-1} + \delta)^2}{(r_{i+1} - \delta)^4} < \infty$$

for each i . Hence, \mathbf{f} is locally Lipschitz; by the Picard-Lindelöf theorem [25], IVP (3.2) has a unique local solution in Ω . This local solution is smooth since \mathbf{f} is smooth.

Let $\mathbf{r}^{in} \in W$ and suppose that $[0, T)$ is a maximal interval on which the problem $\dot{\mathbf{r}} = \mathbf{f}(\mathbf{r}), \mathbf{r}(0) = \mathbf{r}^{in}$ has a solution in W . Since $r_0 = r_0^{in} - t$, we establish that

$$(3.4) \quad T \leq r_0^{in} < \infty.$$

We will show that $\mathbf{r}(t)$ approaches ∂W as $t \uparrow T$. Suppose by contradiction that $\mathbf{r}(t)$ does not approach ∂W as $t \uparrow T$. Then, in particular, we have $\min_i \inf_{t \in [0, T)} r_i(t) > 0$ and \mathbf{f} is uniformly bounded on the image $\mathbf{r}([0, T))$. Thus, $\mathbf{r}(t)$ is Cauchy-continuous. Therefore, by a standard theorem in the theory of ODE [12] which states that an extension of the solution exists at T if $\lim_{t \uparrow T} \mathbf{r}(t)$ exists in W , the (classical) solution can be extended to $[0, T + b)$. This assertion contradicts the maximality of T . We thus conclude that $\mathbf{r}(t)$ approaches ∂W as $t \uparrow T$.

Now, define the set $V_1 = \{\mathbf{x} \in \mathbb{R}^N \mid \exists i \in I \setminus \{0\} \text{ such that } x_i = x_{i-1}\}$ and $V_2 = \partial W \setminus V_1$. Suppose by contradiction that $\mathbf{r}(T) \in V_1$. Let $\{r_j\}_{j \in J}$ be a set consisting of all components of \mathbf{r} such that $r_j(T) = r_{j-1}(T)$. In particular, J is not empty. So let $j_0 \in J$ be the smallest index. Then, $j_0 - 1 \notin J$, which means that $|\dot{r}_{j_0-1}|$ is bounded from below by some $K > 0$ on $[0, T)$. Since $\dot{r}_{j_0-1}(t) \leq 0$ on $[0, T)$, this implies that $\dot{r}_{j_0-1}(t) < -K$. On the other hand, given any $\epsilon > 0$, there exists some interval $(T - c, T)$ on which $\dot{r}_{j_0} = -\frac{r_{j_0} - r_{j_0-1}}{r_{j_0}} > -\epsilon$. By taking $\epsilon = K$, we see that $\frac{d}{dt}(r_{j_0} - r_{j_0-1}) = \dot{r}_{j_0} - \dot{r}_{j_0-1} > -K + K = 0$ on $(T - c, T)$. Hence, $\lim_{t \uparrow T} [r_{j_0}(t) - r_{j_0-1}(t)] \neq 0$ and j_0 cannot be in J . By this contradiction, we conclude that (3.2) has a unique global solution which becomes and remains zero when the trajectory meets the subset $\{r_0 = 0\} \setminus V_1$ of a hyperplane $\{r_0 = 0\}$ at some finite time T . Define $t_0 := T$. Then by the definition of f_0 , $r_0(t) \equiv 0$ for $t \in [t_0, \infty)$. Next, we proceed as in the above argument with the dimension of the solution reduced by 1. Continue this procedure until $\mathbf{r} = 0$. \square

REMARK 3.2. In the above proof, t_n are the step collapse times. For $g = 0$ and conical initial data (i.e., $r_i(0)$ linear with i), we will obtain an explicit solution for the top two steps of ODEs (3.2), with indices $i = n, n + 1$ and $t \in (t_{n-1}, t_n)$. For this special case, the explicit solution indicates that steps do not collide, as verified through our numerics; cf. section 5.2.2.

REMARK 3.3. A direct consequence of Theorem 3.1 is that the discrete slopes M_i remain positive and bounded for any N .

REMARK 3.4. The proof of Theorem 3.1 holds as $N \rightarrow \infty$ (for semi-infinite structure).

A statement about the continuum limit is in order.

COROLLARY 3.5. *If the continuum limit of the solution to IVP (3.2) exists, this limit yields a monotone continuum-scale height for all time $t > 0$ provided the height profile is strictly monotone at $t = 0$.*

In fact, we will verify this last statement for the case of conical initial data through an exact solution of the evolution PDE for the slope (see section 5.2).

3.2. Case with $g > 0$. For nonzero g , the proof for the existence of a unique solution to ODE system (2.12) and the non-crossing property of steps for such a solution is similar to the proof for the case with $g = 0$. However, for $g \neq 0$, $\dot{\mathbf{r}}(t)$ becomes unbounded as $r_j \rightarrow r_{j-1}$ for some j . So, the proof that we provide below holds only when N is finite.

THEOREM 3.6. *Let $N \in \mathbb{N}$ be the initial number of steps and $I = \{0, 1, \dots, N\}$. Consider $\mathbf{r}(t) = (r_0(t), r_1(t), \dots, r_N(t))$ and $\mathbf{f}(\mathbf{r}) = (f_0(\mathbf{r}), f_1(\mathbf{r}), \dots, f_N(\mathbf{r}))$ where*

$$(3.5a) \quad f_i(\mathbf{r}) = -\frac{r_i - r_{i-1}}{r_i} \left\{ 1 + \frac{2g}{3} \left[\psi(r_i, r_{i+1}) - \psi(r_{i-1}, r_i) + \frac{\phi(r_i, r_{i+1}) + \phi(r_{i-1}, r_i)}{r_i^2} \right] \right\} \quad \text{if } r_i \neq 0,$$

$$(3.5b) \quad f_i(\mathbf{r}) = 0 \quad \text{if } r_i = 0.$$

Here, ψ and ϕ are defined by (2.10) and (2.11), respectively; and $r_{-1}(t) \equiv 0$ in the definition of f_0 while $r_{N+1}(t) \equiv 0$ in the definition of f_N . Then, there exists a unique global solution to the IVP

$$(3.6) \quad \dot{\mathbf{r}} = \mathbf{f}(\mathbf{r}), \quad \mathbf{r}(0) = \mathbf{r}^{in}, \quad \mathbf{r}^{in} \in W = \{\mathbf{x} \in \mathbb{R}^N \mid 0 < x_0 < \dots < x_N\}$$

in the domain $\Omega = \{\mathbf{x} = (x_i)_{i \in I} \mid x_i \neq 0, i \in I\}$. Furthermore, this solution stays in W for $t \in [0, t_0)$ and in $W_i = \{\mathbf{x} \in \mathbb{R}^N \mid 0 = x_0 = \dots = x_i, x_{i+1} < \dots < x_N\}$ for $t \in [t_i, t_{i+1})$, where t_i is the time when r_i reaches 0. Here, $0 < t_0 < t_1 < \dots < t_N < \infty$. This solution is smooth for all $t \neq t_0, \dots, t_N$. More precisely, $r_i(t)$ is continuous for all t and is smooth on $[0, t_i)$.

Proof. In the spirit of the proof for $g = 0$, we first prove the existence of a unique local solution to problem (3.6). Observe that each f_i is smooth on W . For each vector $\mathbf{r} \in W$, let $0 < \delta < \min_{i \in I} \{r_i, (r_i - r_{i-1})/4\}$. Then, by recourse to ODEs (2.12), for all $\mathbf{y} \in B^N(\mathbf{r}, \delta)$ we note the following bound in regard to partial derivatives of f_i :

$$(3.7) \quad \left| \frac{\partial}{\partial y_i} \left(\frac{y_i - y_{i-1}}{y_i} \psi(y_i, y_{i+1}) \right) \right|^2 = \left| \frac{2y_i y_{i+1}}{y_i(y_i + y_{i+1})} \frac{1}{(y_{i+1} - y_i)^3} - \left(1 - \frac{y_{i-1}}{y_i}\right) \frac{2y_i y_{i+1}}{(y_i + y_{i+1})^2} \frac{1}{(y_{i+1} - y_i)^3} + 3 \left(1 - \frac{y_{i-1}}{y_i}\right) \frac{2y_i y_{i+1}}{y_i + y_{i+1}} \frac{1}{(y_{i+1} - y_i)^4} \right|^2 \leq K(\delta),$$

where $K(\delta) = \mathcal{O}(1/\delta^3)$ for small δ . In (3.7), we used an inverse triangle inequality, $|y_i - y_{i-1}| \geq |r_i - r_{i-1}| - |y_i - r_i| - |y_{i+1} - r_{i+1}| \geq 2\delta$ in order to obtain a bound for each term; for example, the first term in the right-hand side is bounded by

$\frac{(r_i+\delta)(r_{i+1}+\delta)}{(r_i-\delta)(r_{i+1}-2\delta)} \frac{1}{4\delta^3}$. We omit the details on the rest of partial derivatives for each f_i , since the procedure is similar to the one above. Thus, every $|\nabla f_i|$ is bounded from above by a finite number. Therefore, \mathbf{f} is locally Lipschitz; by the Picard-Lindelöf theorem [25], we assert the existence of a unique local solution to problem (3.6).

Now, as before, let $\mathbf{r}^{in} \in W$ and $[0, T)$ be a maximal interval on which the problem

$$(3.8) \quad \dot{\mathbf{r}} = \mathbf{f}(\mathbf{r}), \quad \mathbf{r}(0) = \mathbf{r}^{in}$$

has a (classical) solution in W . Notice that on W , $\dot{r}_0(t) < \dot{r}_0^{(0)}(t)$ where $r_0^{(0)}(t)$ denotes the first component of the solution for IVP (3.2). Thus, $r_0(t) < r_0^{(0)}(t) = r_0^{in} - t$ and we obtain an upper bound for T :

$$(3.9) \quad T \leq r_0^{in} < \infty.$$

By neglecting the negative terms in (3.5) for each i , we obtain an inequality, viz.,

$$(3.10) \quad \dot{r}_i(t) \leq \frac{C}{(r_i - r_{i-1})^2}, \quad C = 4g/3.$$

We now show that $\mathbf{r}(t)$ approaches ∂W as $t \uparrow T$. Suppose by contradiction that this statement is false. Then, $r_i \rightarrow r_{i-1}$ and the right-hand side of (3.10) is clearly bounded above on $[0, T)$. Hence, $\mathbf{f}(\mathbf{r})$ is uniformly bounded on the image $\mathbf{r}([0, T))$ and, by recourse to the argument given in the proof for the case with $g = 0$, we conclude that $\mathbf{r}(t)$ approaches ∂W as $t \uparrow T$.

Let V_1 and V_2 be the sets defined in the proof for Theorem 3.1. Next, we prove that $\mathbf{r}(t) \rightarrow V_2$ as $t \rightarrow T$. Let $\{r_j\}_{j \in J}$ be a set consisting components of \mathbf{r} such that $r_j(T) = r_{j-1}(T)$. Suppose by contradiction that \mathbf{r} reaches V_1 at time T . In particular, this implies that the set J is nonempty. If, for some $j \in J$, \dot{r}_j grows unbounded in the positive direction near time T yet \dot{r}_{j-1} is bounded above, then $\dot{r}_j - \dot{r}_{j-1} > 0$ on some interval $(T - c, T)$, which contradicts the definitions of T and J . Thus, the desired result follows by this contradiction: \mathbf{r} does not reach V_1 by time T .

Because J is nonempty, there exists the smallest index $j_0 \in J$ and the largest index $j_* \in J$ such that the sequence $j_0, j_0 + 1, \dots, j_* - 1, j_*$ is contained in J . Since $j_0 - 1 \notin J$, we have that $r_{j_0-1} - r_{j_0-2} \rightarrow 0$ and $\psi(r_{j_0-2}, r_{j_0-1})$ is bounded. Thus, the only positive term in $f_{j_0-1}(\mathbf{r})$ is bounded near time T , so $\dot{r}_{j_0-1} = f_{j_0-1}(\mathbf{r})$ is bounded from above in some interval $(T - \tilde{c}, T)$. On the other hand, $j_* + 1 \notin J$ implies that $\psi(r_{j_*}, r_{j_*+1}), \phi(r_{j_*}, r_{j_*+1})$ are both bounded. Also, since $j_* \in J$, we deduce that $\phi(r_{j_*-1}, r_{j_*})$ grows as $(r_{j_*} - r_{j_*-1})^{-2}$ whereas $\psi(r_{j_*-1}, r_{j_*})$ grows as $(r_{j_*} - r_{j_*-1})^{-3}$. Thus, $\dot{r}_{j_*}(t)$ must grow unbounded in the positive direction as $t \rightarrow T$.

Hence, the properties that r_{j_0-1} is bounded and r_{j_*} is unbounded warrant that there exists some $j \in J$ for which \dot{r}_j grows unbounded above for times near T yet \dot{r}_{j-1} is bounded above. We conclude that IVP (3.6) has a unique global solution $\mathbf{r}(t)$ that ends when the trajectory meets a subset $\{r_0 = 0\} \setminus V_1$ of the hyperplane $\{r_0 = 0\}$ at some finite time T . Define $t_0 := T$. By the definition of f_0 , $r_0(t) \equiv 0$ for $t \in [t_0, \infty)$. We proceed as in the above argument with a new problem in which the dimension of the solution is reduced by 1. Continue this procedure until $\mathbf{r} = \mathbf{0}$. \square

REMARK 3.7. The above proof relies on the fact that J is a finite set and there exists the largest index in J (i.e., J is bounded). In particular, it is necessary that N be finite. Thus, we may not use our proof for nonzero g in order to assert positivity of the slope for a semi-infinite structure (as $N \rightarrow \infty$).

REMARK 3.8. For nonzero g , one can state a result analogous to Corollary 3.5.

4. Formal continuum limit outside facet. In this section, we review the derivation of PDEs for the surface height and slope profiles away from the facet on the basis of the step velocity law (2.12). Our computations are formal, primarily invoking notions of pointwise convergence (with the exception of (4.6) for μ); similar, yet more detailed, heuristic derivations are presented in [38, 40] as parts of the (technically more involved) case with surface diffusion in 2D, where the step velocity is the difference of adatom fluxes each of which is expressed in terms of differences of step chemical potentials of neighboring terraces. We emphasize that the derived continuum laws are valid only for $r > r_f(t)$. The a priori unknown facet position, $r_f(t)$, should be determined from solving a free boundary problem (see section 5).

Consider $N \gg i \gg n \gg 1$ with $ia = \mathcal{O}(1)$, in view of (2.3). We assume that the discrete slopes, M_i , are kept fixed; cf. (2.1). On each terrace, $r_{i-1} < r < r_i$, we have $h_d(r, t) = \text{const.}$; as $r \uparrow r_i(t)$, the differentiation of $h_d(r, t)$ with respect to time yields

$$(4.1) \quad \dot{r}_i \rightarrow \partial_t h(r, t)/m(r, t)|_{r=r_i(t)} \quad \text{as } a \rightarrow 0,$$

where $m(r, t) = -\partial_r h(r, t)$ and $r > r_f(t)$. Equation (4.1) reveals the limit of the right-hand side of (2.12).

On the other hand, the discrete mobility, $\nu_i = \nu(r_i - r_{i-1})/a$, approaches

$$(4.2) \quad \nu_i \rightarrow \nu/m(r, t)|_{r=r_i(t)}, \quad r > r_f(t).$$

Thus, if $\mu_i(t) \rightarrow \mu(r, t)$, the continuum-scale chemical potential, (4.1) and (4.2) yield

$$(4.3) \quad \partial_t h(r, t) = -\nu\mu(r, t) \quad r > r_f(t).$$

There are at least two routes to obtaining a formula for μ . One way is to directly take the limit of (2.9) under the condition $\mathcal{O}(a) = r_i - r_{i-1} \ll r_i$ for large i . For this purpose, the right-hand side of (2.9) is expressed in terms of discrete slopes, M_i , with the main substitution

$$r_{i\pm 1} \sim r \pm \frac{a}{m(r, t)}, \quad r = r_i.$$

The algebraic manipulations of this procedure are detailed in [38] (see also [30]). The resulting formula reads [38]

$$(4.4) \quad \mu(r, t) = \frac{\Omega g_1}{r} + \Omega g_3 \frac{1}{r} \frac{\partial}{\partial r} (r m^2), \quad r > r_f(t).$$

Alternatively, by (2.5) and (2.8) one can write $\mu(r, t)$ as the first variation of the continuum limit of $E^{\text{st}}(t; a)$. In view of the coarea formula $\sum_i a \oint_{L_i} \cdot ds \rightarrow \int |\nabla h| \cdot dA$ [40], this limit is the well-known surface free energy [24]

$$(4.5) \quad E^{\text{st}} \xrightarrow{a \rightarrow 0} E(h) = \iint \left(g_1 |\nabla h| + \frac{g_3}{3} |\nabla h|^3 \right) dA,$$

where $dA = dx dy$ and integration is carried out on the crystal reference (“basal”) plane. The free energy density $\gamma(|\nabla h|) \equiv g_1 |\nabla h| + (g_3/3) |\nabla h|^3$ is manifestly singular at the zero slope surface orientation, $\nabla h = 0$, which defines the facet. Now, μ is obtained through [38, 40]

$$(4.6) \quad \langle \mu, \partial_t h \rangle = \Omega \dot{E} \Rightarrow \mu(r, t) \equiv \Omega \frac{\delta E}{\delta h}, \quad r > r_f(t),$$

where $\langle \mu, \varphi \rangle = \iint \mu(x, y) \varphi(x, y) dA$ denotes the usual L^2 -inner product, and $\delta E / \delta h$ is the variational derivative of $E(h)$. Equation (4.6) is consistent with continuum thermodynamics and is valid outside the facet. The use of (4.5) and integration by parts lead to (4.4).

Equations (4.3) and (4.4) yield a PDE for the height,

$$(4.7) \quad \partial_t h = -\nu \Omega g_1 \operatorname{div} \boldsymbol{\xi}, \quad r > r_f(t),$$

where the radial vector $\boldsymbol{\xi}$ is

$$(4.8) \quad \boldsymbol{\xi} = \xi e_r, \quad \xi(r, t) = 1 + gm(r, t)^2,$$

and e_r is the unit radial vector. The PDE for the positive slope, $m = -\partial_r h > 0$, outside the facet is

$$(4.9) \quad \partial_t m = -\nu \Omega g_1 \{r^{-2} - g \partial_r [r^{-1} \partial_r (rm^2)]\}.$$

It is worthwhile noting that (4.7) has the form of a mass conservation statement, where $\boldsymbol{\xi}$ plays the role of a vector-valued flux associated with $\partial_t h$. This observation will later enable us to interpret a boundary condition at the facet via notions of shock wave theory (see section 6.1).

5. Computations for surface profile. In this section, we describe continuum solutions for the height and slope profiles and make comparisons to discrete simulations. For this purpose, we invoke elements of the subgradient theory [33] in order to pose a free boundary problem for the facet [59]. We then solve the free boundary problem for (4.9) for $g = 0$ (non-interacting steps) and $0 < g \ll 1$; in the latter case, we apply boundary layer theory in the spirit of [38]. For $g > 0$, we solve numerically PDE (4.9) for the slope profile by assuming self-similarity.

5.1. Formulation of boundary conditions. As mentioned above, within the continuum framework, there are at least two approaches to facet evolution: the subgradient formulation, which replaces the PDE outside the facet by a statement of variational nature everywhere; and the free boundary approach. The two approaches can of course be made compatible if the boundary conditions at the facet edge (free boundary) are chosen to be appropriate natural boundary conditions resulting from the subgradient theory. In this section, we start with the subgradient formulation in order to indicate the corresponding boundary conditions. Furthermore, we entertain the scenario of replacing one of these conditions with a statement about the facet speed, which can in principle incorporate discrete effects.

5.1.1. Elements of subgradient and free boundary approaches. A guiding principle in the analysis of the continuum law (4.6) is that the height profile evolves so that the energy, $E(h)$, decreases most rapidly [47]. Note that (4.6) is ill-defined on the facet due to the singularity of $E(h)$ at $\nabla h = 0$. We invoke the extended gradient theory to circumvent this difficulty [33].

The main idea stemming from the extended gradient formulation (reviewed in Appendix A.1) is to state the evolution law for h in the form (4.7) *everywhere*, including the facet. Thus, (4.7) is replaced by the statement

$$(5.1) \quad \partial_t h(r, t) = -\nu \Omega g_1 \operatorname{div} \boldsymbol{\xi}(r, t) \quad \text{for all } r \geq 0,$$

where $\operatorname{div} \boldsymbol{\xi}$ is expressed in terms of $\delta E / \delta h$ *only* outside the facet. The flux $\boldsymbol{\xi}$ is uniquely determined from (5.1) under the assumption of sufficient regularity; in addition, the

subgradient formulation with the energy density $g_1^{-1}\gamma(|\nabla h|) = |\nabla h| + g|\nabla h|^3$ asserts that $|\boldsymbol{\xi}| \leq 1$ on the facet (see Appendix A.1) [33].

Equation (5.1) states that there is mass conservation globally for the height, h . Hence, by the continuity of h (a necessary condition for any physical situation), it is reasonable to impose continuity of $\boldsymbol{\xi}$ [33, 59]. In other words, if $\boldsymbol{\xi}$ were discontinuous, the finite speed of the free boundary (facet edge) would imply that h exhibits a jump across the facet edge. These statements are placed on firmer ground in Appendix A.1.

Next, we write down explicit boundary conditions for (4.7). Note that four (three) conditions are needed, since the PDE for h is of second (first) order for $g > 0$ ($g = 0$), and $r_f(t)$ and $h_f(t)$ are (a priori unknown) parts of the solution. If $r < r_f(t)$ then $h = h_f(t)$. By continuity of height, we write

$$(5.2) \quad h_f(t) = h(r, t) \quad \text{as } r \downarrow r_f(t).$$

Equation (5.1) on the facet reads $\dot{h}_f = -\nu\Omega g_1 r^{-1} \partial_r(r\xi)$, by which $\nu\Omega g_1 \xi = -(r/2)\dot{h}_f + C(t)/r$ if $r < r_f(t)$; $C(t) \equiv 0$ so that ξ be bounded. Thus, continuity of $\boldsymbol{\xi}(r, t)$ entails

$$(5.3) \quad -\frac{r_f(t)}{2} \dot{h}_f = \nu\Omega g_1 [1 + gm(r, t)^2], \quad \text{as } r \downarrow r_f(t).$$

On the other hand, for large r , the solution must be compatible with the prescribed initial data:

$$(5.4) \quad h(r, t) \sim h(r, 0); \text{ or } m(r, t) \sim -\partial_r h(r, 0), \quad \text{as } r \rightarrow \infty,$$

which is a ‘‘far field’’ condition.

For $g > 0$, one more condition must be imposed. Recall that $|\boldsymbol{\xi}| \leq 1$ on the facet (as explained in Appendix A.1), $\xi = 1 + gm^2 > 1$ outside the facet ($r > r_f(t)$), and ξ is continuous. Thus, the slope is continuous at $r = r_f(t)$:

$$(5.5) \quad m(r_f, t) = 0.$$

Equations (5.2)–(5.5) form the desired set of conditions for PDE (4.7) in the facet free boundary problem. In view of (5.5), the differentiation of (5.2) with respect to t can be used to replace (5.2) and (5.3) by a single condition via elimination of \dot{h}_f .

5.1.2. Alternate boundary condition: step collapses. Next, we address the following scenario. Suppose that we need to inject information about step collapses into the continuum theory. We now show that this information can be recast to an approximation for the speed, $-\dot{h}_f$, of the facet. In the spirit of [39], we entertain the idea of using this approximation in the place of the continuity of $\boldsymbol{\xi}$. In section 5.2.2, we numerically show that this modified boundary condition turns out to be consistent with the flux ($\boldsymbol{\xi}$) continuity for our model (section 5.1.1).

The starting point is to require that the facet height decrease by multiples of a [30, 39], while keeping intact the surface height and slope continuity (for $g > 0$), and the far field condition. We thus impose the relation [30, 39]

$$(5.6) \quad h_f(t_{n-1}) - h_f(t_n) = a.$$

To extract a statement for $\dot{h}_f(t)$, we view t_n as the (continuous) time, t , for large enough n . By Taylor-expanding (5.6) at $t = t_n$, we obtain [39]

$$(5.7) \quad -\dot{h}_f(t) \approx \frac{a}{\delta t(t)},$$

which relates the speed $-\dot{h}_f$ with the differences, $\delta t(t) = t_n - t_{n-1}$, of step collapse times. Here, we heuristically set $n \approx \mathbf{n}(t)$ via $t_n \approx t$ if $n \gg 1$; for instance, if $t_n \sim cn^B$ then $n \approx \mathbf{n}(t) = c^{-1/B}t^{1/B}$ and thus $\delta t(t) \sim \beta cn^{B-1} \approx \beta c^{1/B}t^{(B-1)/B}$.⁵ Note that we must assume $t_n \gg 1$ so that $t_n - t_{n-1} \ll t_n$, which is needed for the Taylor expansion to make sense.

Next, we relate $\delta t(t)$ with the derivative of m^2 at $r = r_f$. Suppose $g > 0$. By differentiating (5.2) we have $\dot{h}_f(t) = -m(r_f, t)\dot{r}_f + \partial_t h = \partial_t h$ as $r \downarrow r_f(t)$ via (5.5) for finite \dot{r}_f . Thus, in view of PDE (4.7), relation (5.7) becomes

$$(5.8) \quad \nu\Omega g_1 [1 + g\partial_r(rm^2)]|_{r \downarrow r_f(t)} \sim r_f(t) \frac{a}{\delta t(t)},$$

for large enough t (and n).

The case with $g = 0$ is special, because m is not continuous at $r = r_f$; cf. (5.22) of section 5.2. The relation $\dot{h}_f = -m\dot{r}_f + \partial_t h$ as $r \downarrow r_f$ now implies

$$(5.9) \quad \nu\Omega g_1 + m_f \dot{r}_f r_f(t) \sim r_f(t) \frac{a}{\delta t(t)}, \quad m_f = \lim_{r \downarrow r_f} m,$$

for large t ; notice the appearance of the term $m_f \dot{r}_f r_f$ on the left-hand side.

Equations (5.8) and (5.9) would in principle require input from discrete (step) simulations for $\delta t(t)$ if these conditions aimed to replace the continuity of ξ , condition (5.3). Then, the boundary conditions would finally be (5.2), (5.4), (5.5), and (5.8) for $g > 0$; or, (5.2) and (5.9) for $g = 0$.

REMARK 5.1. Alternatively, suppose that we retain the continuity of ξ and seek an approximate formula for $\delta t(t)$ accordingly. By (5.3), (5.5) and (5.6), we obtain

$$(5.10) \quad \delta t(t) \approx \frac{a}{2\nu\Omega g_1} r_f(t),$$

which is applied for large enough t and all finite $g \geq 0$ (with $g_1 > 0$). In section 5.2.2, we show that for our ad hoc model M1, (5.10) yields a prediction for t_n in agreement with the discrete simulations for large n .

Initial data. In the remainder of this article, to simplify analytical and numerical computations, we consider an initial conical profile of unit slope, viz.,

$$(5.11) \quad h(r, 0) \equiv h_0(r) = \begin{cases} h_{f0}, & r < r_{f0}, \\ h_{f0} - (r - r_{f0}), & r > r_{f0}, \end{cases}$$

where $r_{f0} = r_f(0)$ and $h_{f0} = h_f(0)$. This profile corresponds to the initial step train

$$(5.12) \quad r_i(0) = r_{f0} + ia,$$

where the top layer is located at height h_{f0} .

5.2. Case with zero step interaction ($g = 0$). We now describe the continuum-scale height and slope profiles stemming from the thermodynamics approach (section 5.1.1) in the special case without step-step interaction, $g = 0$. In this case, the continuity of slope, equation (5.5), is *not* necessarily applicable. The resulting formula for $m(r, t)$ exhibits a self-similar behavior, which we verify by discrete simulations. This finding motivates the computations of sections 5.3 and 5.4. For algebraic convenience, in the remainder of section 5 we employ units with $\nu\Omega g_1 = 1 = a$.

⁵We loosely use the symbol \approx to state that an integer, here n , is approximated by a continuous variable in some appropriate (yet not precisely defined here) sense when n is large.

5.2.1. Exact continuum solution. For $g = 0$, PDE (4.7) reduces to

$$(5.13) \quad \partial_t h = -\frac{1}{r}, \quad r > r_f(t),$$

which has the general solution

$$(5.14) \quad h(r, t) = h_0(r) - \frac{t}{r}, \quad r > r_f(t).$$

It remains to compute the facet radius, $r_f(t)$.

The differentiation of (5.2) with respect to t under initial data (5.11) entails

$$(5.15) \quad \dot{h}_f(t) = -\dot{r}_f(t) - \frac{1}{r_f(t)} + \frac{t}{r_f(t)^2} \dot{r}_f(t).$$

On the other hand, the continuity of ξ , (5.3), yields

$$(5.16) \quad -\frac{r_f(t)}{2} \dot{h}_f = 1.$$

Equations (5.15) and (5.16) lead to

$$(5.17) \quad \dot{r}_f = \frac{r_f}{r_f^2 - t}, \quad r_f(0) = r_{f0},$$

which can be solved exactly via inversion, $t = T(r_f)$: $t = T(r_f) = -(r_{f0}^3/3)r_f^{-1} + r_f^2/3$. Thus, $r_f(t)$ satisfies $r_f^3 - 3tr_f - r_{f0}^3 = 0$ and turns out to be equal to [4] $r_f(t) = [r_{f0}^3/2 + \vartheta(t)]^{1/3} + [r_{f0}^3/2 - \vartheta(t)]^{1/3}$ where $\vartheta(t) = \sqrt{r_{f0}^6/4 - t^3}$ (the positive square root is taken for $t < 2^{-2/3}r_{f0}^2$). For $t > 2^{-2/3}r_{f0}^2$, the solution for r_f reads

$$(5.18) \quad r_f(t) = 2\sqrt{t} \cos\left(\frac{1}{3} \tan^{-1} \frac{\sqrt{4t^3 - r_{f0}^6}}{r_{f0}^3}\right).$$

By (5.18), we compute

$$(5.19) \quad r_f(t) \sim \sqrt{3t} \quad \text{as } t \rightarrow \infty.$$

Once $r_f(t)$ is evaluated, $h_f(t)$ follows via continuity of height, $h_f(t) = h_{f0} + r_{f0} - r_f - t/r_f$; in particular,

$$(5.20) \quad h_f(t) \sim h_{f0} + r_{f0} - \frac{4}{\sqrt{3}}\sqrt{t} \quad \text{as } t \rightarrow \infty.$$

By (5.14), the surface slope profile is

$$(5.21) \quad m(r, t) = 1 - \frac{t}{r^2}, \quad r > r_f(t); \quad m \equiv 0, \quad r < r_f(t).$$

Clearly, this slope has the form $m(r, t) = \mathbf{m}(\eta)$ with self-similarity variable $\eta = r/\sqrt{t}$. By (5.19), we note that

$$(5.22) \quad m(r, t) \rightarrow m_f := \mathbf{m}(\sqrt{3}) = \frac{2}{3} \quad \text{as } r \downarrow r_f(t), \quad t \rightarrow \infty;$$

interestingly, the slope is *discontinuous* at the facet edge.

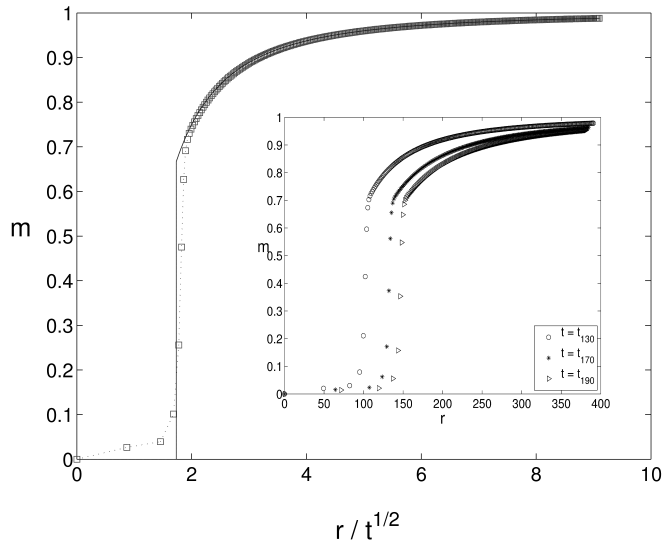


FIG. 5.1. *Exact continuum slope $m(r,t)$ (solid line) and discrete slopes M_i (symbols) as functions of r/\sqrt{t} (where $r = r_i$) for $g = 0$ and initial cone of unit slope with $N = 400$ steps. The slope $m(r,t)$ is computed from (5.21) and (5.18); and $M_i(t)$ are obtained at $t = t_n$ by numerically solving (2.12). The vertical line indicates the (continuum-scale) facet position, $\eta_F = r_f(t)/\sqrt{t} \approx \sqrt{3}$. Inset shows corresponding simulation data for M_i versus r_i at different collapse times $t = t_n$.*

5.2.2. Numerical solution. To compare (5.18) and (5.21) to the discrete step flow for non-interacting steps, we numerically solve (2.12) for $g = 0$ under initial data (5.12) and compute the corresponding discrete slopes, $M_i = 1/(r_{i+1} - r_i)$; see Appendix B where we exactly determine the positions of the two top steps for validation purposes. In Figure 5.1, we plot simulation data for M_i versus r_i at different times $t = t_n$, and observe that the data collapse to a single graph if r_i is scaled by \sqrt{t} . Figure 5.1 shows that the numerically computed $M_i(t)$ follow closely the exact $m(r,t)$.

It is of interest to estimate the step collapse times, t_n , and their differences $t_n - t_{n-1}$ for $n \gg 1$ via (5.19) and (5.21) with recourse to Remark 5.1, particularly (5.10), for $t \gg 1$ (with $\nu\Omega g_1 = 1$). Thus, we obtain $\delta t(t) \sim \sqrt{3t}/2$, by which $t_n \sim cn^\beta$ with $\beta = 2$ and $c = 3/16$. In Figure 5.2, the collapse times t_n are plotted versus n ; the above scaling law including the prefactor c are thus verified by our numerics. This observation about t_n provides some additional evidence that, for $g = 0$, the subgradient-based boundary conditions are consistent with the discrete step flow; and, in particular, the continuum version of step collapses, condition (5.9), is compatible (and hence can replace) the continuity of ξ .

5.3. Self-similar slopes for $g > 0$. In this section, we study PDE (4.9) via numerics for arbitrary $g > 0$ under the assumption that the slope is self-similar at long time. We are motivated by (i) the exact solution of section 5.2, where we found $m(r,t) = m(\eta)$ with $\eta = r/\sqrt{t}$ and $r_f(t) \sim \sqrt{3t}$ for $t \gg 1$, and (ii) numerical computations for $M_i(t)$. Our task is to reduce the evolution PDE for $m(r,t)$ to an ODE; solve this ODE numerically for $g > 0$ with boundary conditions from the subgradient formulation (section 5.1.1); and compare the continuum predictions to simulations for discrete slopes. The possibility and nature of self-similarity in our

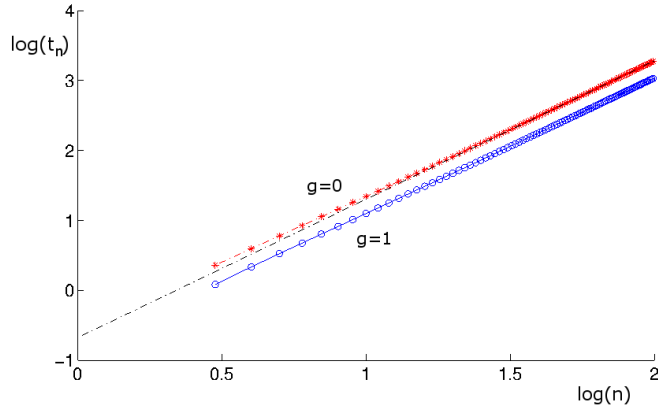


FIG. 5.2. Log-log plot of step collapse times t_n versus n for $g = 0$ (asterisks) and $g = 1$ (circles), numerically computed from (2.12) for initial cone of unit slope. The dot-dashed (straight) line indicates the numerically computed large- n asymptotic behavior of t_n for $g = 0$. The scaling law $t_n \sim cn^\beta$ is verified for $n \gg 1$ with $\beta \approx 2$ for $g = 0, 1$. For $g = 0$, we find $c = 0.1879 \approx 3/16$, in close agreement with the prediction of section 5.2.2.

radial setting is not clarified analytically here.

First, we provide some numerical evidence that the discrete slopes have an apparently self-similar structure for large enough time: In Figure 5.3 (inset) we plot M_i versus r_i for $g = 1$ at different times, $t = t_n$; and observe the data collapse once r_i is scaled with \sqrt{t} , which indicates self-similarity.

Next, we simplify PDE (4.9) by setting $m(r, t) = \mathbf{m}(\eta)$, $\eta = r/\sqrt{t}$, for arbitrary $g > 0$. By use of the similarity variable η , the facet position is $\eta_f = r_f(t)/\sqrt{t} \sim \sqrt{3}$. Thus, PDE (4.9) is converted to an ODE for $\mathbf{m}(\eta)$:

$$(5.23) \quad -\frac{1}{2}\eta\mathbf{m}'(\eta) = -\eta^{-2} + g[\eta^{-1}(\eta\mathbf{m}^2)']' \quad \eta > \eta_f ;$$

the prime denotes differentiation with respect to the argument, here η . By elimination of \dot{h}_f in (5.2)–(5.5), we wind up with the boundary conditions

$$(5.24) \quad g(\eta\mathbf{m}^2)' = 1, \quad \eta \downarrow \eta_f,$$

$$(5.25) \quad \mathbf{m}(\eta) \rightarrow 1, \quad \eta \rightarrow \infty,$$

$$(5.26) \quad \mathbf{m}(\eta) = 0, \quad \eta \downarrow \eta_f .$$

Note that there are three boundary conditions for a second-order ODE, because (the unknown) η_f is a part of the solution. We have not been able to analytically solve (5.23)–(5.26), and hence proceed to find a numerical solution. We assume (but not prove) that $\mathbf{m}(\eta) \geq 0$ for $\eta \geq \eta_f$.

5.3.1. Numerical solution. To solve the (free) boundary value problem of (5.23)–(5.26), we first apply a transformation of (η, \mathbf{m}) that (i) maps (η_f, ∞) to a finite interval, and (ii) renders linear the highest-order derivative in ODE (5.23) [17, 19].

So, we apply a simple translation, $s = \eta - \eta_f$. This maps (η_f, E) to $(0, \check{E} = E - \eta_f)$ where $E \gg \eta_f$ is a large number that replaces infinity. In addition, we convert ODE (5.23) to a system of first-order ODEs for the variables $\mathfrak{M}_1(s) = \mathbf{m}^2(\eta)$ and

$\mathfrak{M}_2(s) = (\mathfrak{m}^2)'(\eta)$. The resulting system reads

$$\begin{aligned} \mathfrak{M}'_1(s) &= \mathfrak{M}_2(s), \\ \mathfrak{M}'_2(s) &= \frac{1}{g} \left[-\frac{1}{4}(s + \eta_f)\mathfrak{M}_1^{-1/2}\mathfrak{M}_2 + (s + \eta_f)^{-2} \right] \\ &\quad + (s + \eta_f)^{-2}\mathfrak{M}_1 - (s + \eta_f)^{-1}\mathfrak{M}_2, \end{aligned}$$

along with boundary conditions at $s = 0$ (facet edge) and $s = \check{E}$ obtained from (5.24)–(5.26); in particular, $\mathfrak{M}_1(\check{E}) = 1$. To find a numerical solution, we seek an expansion of \mathfrak{M}_1 in powers of s according to⁶

$$(5.27) \quad \mathfrak{m}(\eta) = \mathfrak{M}_1(s)^{1/2} \sim \sum_{l=1}^k c_l s^{l/2} =: S_k(s),$$

which satisfies condition (5.26). By (5.24), we compute $c_1^2 = (g\eta_f)^{-1}$. The remaining coefficients, c_l (for $l = 2, \dots, k$), are found via dominant balance in (5.23); notice that $c_l = c_l(\eta_f)$ for $l \geq 1$. Then, we evaluate $\mathfrak{M}_1(s)$ at a fixed point s_0 near 0 in terms of η_f , and apply an iterative algorithm (e.g., the `bvp4c` Matlab routine [29]) based on a suitable initial guess for $\mathfrak{M}_1(s)$ that aims to satisfy $\mathfrak{M}_1(\check{E}) = 1$. In Appendix C, we provide the coefficients c_l for $l \leq 13$; this helps evaluate the S_k of (5.27) for $k = 13$.

A satisfactory initial guess for $\mathfrak{M}_1(s)$, which apparently causes our numerical scheme to converge to a reasonable slope profile, is constructed through boundary layer theory [38]. Although this theory is in principle valid for $0 < g \ll 1$, we apply it for g that is not small, e.g., $g = 1$, as a means of obtaining an initial guess for the slope within our numerical scheme; see section 5.4 for the formal boundary layer analysis.

In Figure 5.3, we plot the discrete slopes M_i and continuum slope m versus r/\sqrt{t} for $g = 0.1$ and 1, demonstrating the agreement of step simulations and macroscopic (subgradient-based) predictions.

REMARK 5.2. The facet size is expected to be monotonically decreasing with $g = g_3/g_1$ at fixed time t [39]. Physically, this effect can be attributed to the tendency of steps to cover a larger part of the surface if their repulsion (g_3) increases or their self-energy (line tension, g_1) decreases. As a result, in principle any microscale events on top of the facet, e.g., collapses of individual steps, are expected to be more pronounced for smaller g (see, e.g. [39] for a model of diffusion limited kinetics).

REMARK 5.3. The self-similar behavior of the slope profile implies a scaling law for the step collapse times, t_n . By (5.8), we find $t_n - t_{n-1} = \delta t(t) \sim c(g)\sqrt{t}$ for some g -dependent constant c , and thus $t_n \sim c^2 n^2/4$ for $n \gg 1$ (cf. Figure 5.2 for $g = 1$). This $c(g)$ should decrease with g since stronger step repulsions should cause steps to shrink faster on top of the facet [39]. By Figure 5.2, we find numerically (via discrete simulations) a value for c consistent with condition (5.10).

5.4. Boundary layer theory, $0 < g \ll 1$. In this section, we apply boundary layer theory in order to construct a solution to the free boundary problem described by (4.9) and (5.2)–(5.5) when $0 < g \ll 1$ [28, 38]. The main observation is that by setting $g = 0$ in the evolution PDE (4.9) it is impossible to obey the continuity of slope, (5.5). So, we split the domain outside the facet into two regions: an “outer”

⁶We alert the reader that expansion (5.27) is postulated. This expansion is consistent with the structure of the evolution PDE; and it is partly motivated by an expansion of the same form derived systematically via iterations of integral equations in [41] for evaporation dynamics of a 1D step train connecting two semi-infinite facets. We do not pursue a rigorous justification for (5.27) at this stage.

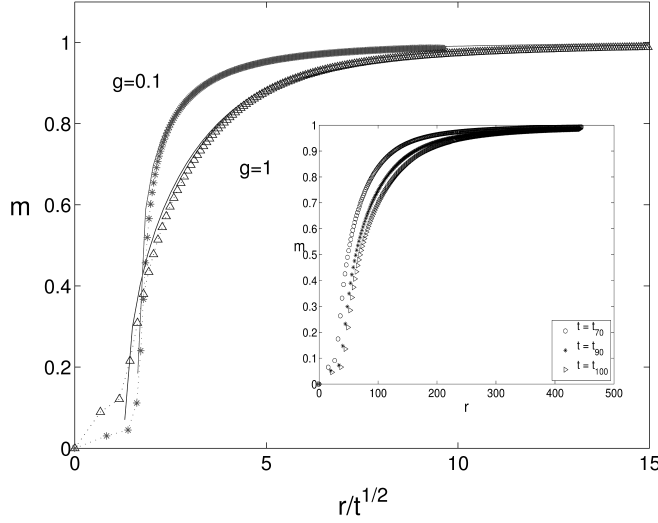


FIG. 5.3. Continuum slope $m(r,t)$ (solid line) and discrete slopes M_i (symbols) as functions of r/\sqrt{t} for initial cone of unit slope; $g = 0.1$ (asterisks) and $g = 1$ (triangles). The slope $m(r,t)$ is computed from numerically solving (5.23)–(5.26); and $M_i(t)$ are determined from (2.12). Inset shows discrete slopes M_i versus position $r = r_i$ at distinct times $t = t_n$ for $g = 1$; the data collapse to the graph of main figure.

region, in which the step self-energy (line tension) dominates over the step interaction energy; and the “inner” region (boundary layer), in which the step interaction energy is significant [38]. The width of the boundary layer scales with a positive power of g (cf. (5.28)). Inside the boundary layer, the slope m should vary smoothly from its zero value ($m = 0$) at the facet edge to the behavior predicted for $g = 0$ in the outer region, ; cf. (5.21). The outer solution should be compatible with the continuity of height and flux, and the far field condition. Hence, we only need to compute the inner solution by imposing zero slope at the facet edge.

For later algebraic convenience, we set [38]

$$(5.28) \quad m(r,t) = a_0(t)f_0(\zeta,t), \quad \zeta = \frac{r - r_f(t)}{g^\alpha w(t)},$$

where $g^\alpha w(t)$ measures the (a priori unknown) width of the boundary layer and α is a suitable exponent (to be determined); the amplitude $a_0(t)$ will be chosen via the matching of inner and outer solutions; and (for ease of notation) $r_f(t) \equiv r_f(t; g = 0)$ denotes the facet radius for $g = 0$ (see, e.g. (5.18)). The substitution of (5.28) into (4.9) yields

$$\begin{aligned} & \dot{a}_0 f_0 + a_0 \partial_t f_0 - g^{-\alpha} \frac{a_0}{w} (\dot{r}_f + g^\alpha \dot{w} \zeta) \partial_\zeta f_0 \\ &= - \frac{1}{(r_f + g^\alpha w \zeta)^2} + g^{1-2\alpha} \frac{a_0^2}{w^2} \\ & \quad \times \partial_\zeta \left\{ (r_f + g^\alpha w \zeta)^{-1} \partial_\zeta [(r_f + g^\alpha w \zeta) f_0^2] \right\}. \end{aligned}$$

By treating ζ as well as a_0 , f_0 , w , r_f and their derivatives as $\mathcal{O}(1)$, we observe that

the $\mathcal{O}(g^{-\alpha})$ term on the left-hand side of the last equation must be balanced by the $\mathcal{O}(g^{1-2\alpha})$ term on the right-hand side; thus, $\alpha = 1$.

The resulting equation for f_0 reads

$$(5.29) \quad \partial_{\zeta\zeta}(f_0^2) = -\ell\partial_{\zeta}f_0, \quad \zeta > 0; \quad \ell = w\dot{r}_f/a_0.$$

By matching $a_0(t)f_0(\zeta, t)$ as $\zeta \rightarrow \infty$ and $r \downarrow r_f(t)$ with the outer solution for m given by (5.21), we take

$$(5.30) \quad a_0(t) = 1 - \frac{t}{r_f(t)^2}$$

while we set

$$(5.31) \quad f_0 \rightarrow 1 \quad \text{as } \zeta \rightarrow \infty.$$

By integrating (5.29), in view of (5.31), we obtain

$$(5.32) \quad (f_0^2)_{\zeta} = \ell(1 - f_0), \quad \zeta > 0; \quad f_0 \rightarrow 0 \quad \zeta \downarrow 0,$$

where we imposed the condition of vanishing slope at the facet. We henceforth consider $\partial_t f_0 \equiv 0$ and set $\ell = \text{const}$. By solving (5.32) we obtain $2f_0 + \ln(1 - f_0) = -\ell\zeta$, which must be compatible with (5.31). Thus, $\ell > 0$; without loss of generality, set $\ell = 1$. Accordingly, the solution f_0 satisfies the transcendental equation

$$(5.33) \quad f_0(\zeta) = 1 - e^{-\zeta/2}e^{-f_0(\zeta)}, \quad \zeta > 0.$$

It is of some interest to point out that f_0 is given by

$$(5.34) \quad f_0(\zeta) = 1 + W(\varsigma(\zeta)), \quad \varsigma(\zeta) = -e^{-1-\zeta/2},$$

where $W(x)$ is the Lambert function [13]. By the definition of ℓ , equation (5.29), we find the width

$$(5.35) \quad w(t) = \frac{a_0(t)}{\dot{r}_f(t)} = \dot{r}_f(t)^{-1} \left[1 - \frac{t}{r_f(t)^2} \right].$$

This finding concludes our computation of the inner solution for m . Formulas (5.30) and (5.35) can be simplified for $t \gg 1$ which entails $r_f(t) \sim \sqrt{3t}$.

REMARK 5.4. A composite solution, which accounts for both the inner and outer solution, can be formally constructed by adding the slope of (5.21) to $a_0(t)f_0(\zeta)$ and subtracting their common limit [28]:

$$(5.36) \quad m(r, t) \sim 1 - \frac{t}{r_f(t)^2} + a_0(t)[f_0(\zeta) - 1], \quad r > r_f(t),$$

where $r_f(t)$, $a_0(t)$ and $f_0(\zeta)$ are given by (5.18), (5.30) and (5.34).

6. Discussion. In this section, we make an attempt to offer more insight into our model M1. First, we discuss the compatibility of the subgradient formulation with notions of shock wave theory. This point of view is heuristic. In this context, an unconventional definition of the facet is introduced by invoking elements of shock waves [64]. This interpretation of the facet aims to provide some physical intuition about the character of the continuum theory for our model. Second, we discuss two more physically transparent models (M2 and M3) derived as a special case of surface diffusion in the BCF framework; M1 follows from simplification of these models. For $g = 0$, we show by numerics that the discrete dynamics of one of these models (M2) apparently respect self-similarity but are not consistent with the corresponding subgradient theory.

6.1. Shock wave interpretation and facet definition. Next, we provide a connection of facet motion with shock waves, by interpreting the continuity of flux ξ , condition (5.3), as a statement for the speed of the facet boundary viewed as a shock. This viewpoint aims to render more transparent the relation of the continuum (subgradient) theory to step flow, and was recently invoked in a study of surface diffusion [19]. The shock wave picture is deemed appealing, especially because it bears some analogy with a kinematic description of step motion by Cabrera, Frank and Vermilyea [9, 20].

The shock wave notion emerges naturally in Lagrangian coordinates of motion [18, 19], i.e., the step radius and the surface height, which are treated as the dependent and independent continuum variables respectively. Thus, set $r_i(t) \equiv R(\chi_i, t)$ where $\chi_i = ia$ becomes the continuous variable $\chi = h_f(0) - h = \mathcal{O}(1)$ as $a \rightarrow 0$ (in the macroscopic limit). Hence, (2.12) reduces to a PDE for R . This PDE is recast to

$$(6.1) \quad \partial_t(R^2) + 2\nu\Omega g_1 \partial_\chi \left[R \left(1 + g(\partial_\chi R)^{-2} \right) \right] = 0,$$

outside the facet, $\chi > \chi_f(t) = h_f(0) - h_f(t)$. Note the relation $(\partial_\chi R)^{-1} = m$ and the fact that the continuity of h is inherent in the use of χ as a continuous variable. Equation (6.1) reads as the volume conservation law $\partial_t \varrho + \partial_\chi J = 0$ with “density” $\varrho = \pi R^2$ (area of a layer) and “flux” $J = (2\pi R) \nu \Omega g_1 [1 + g(\partial_\chi R)^{-2}]$. For $g = 0$, (6.1) becomes a simple kinematic, traffic-flow-type, equation. This form of PDE is known to develop shock wave solutions [64]. Here, we heuristically extend the shock wave notion to the present case with a facet and $g > 0$. However, it is compelling to point out some subtleties: *By contrast* to typical traffic flow situations, PDE (6.1) is (i) of second order for $g > 0$ and (ii) *not* valid on one side of the facet edge (viewed as a shock in the (χ, t) plane). We are aware that, despite the possible intuition gained by this formalism in the context of the continuum theory, the shock wave picture based on (6.1) so far does not convey any information about how *steps* actually behave as $a \rightarrow 0$. In other words, the issue of convergence from the discrete to a continuum solution is not clarified here.

We give the following alternate definition of the facet boundary at $r = r_f(t)$. Then, we point out that the shock wave theory using this definition of the facet is compatible with the subgradient theory.

DEFINITION 6.1. *Define the facet so that at the facet edge ($\chi = \chi_f$) each of the variables ϱ and J has a jump discontinuity. Specifically, in the direction of decreasing χ , these variables decrease from the values $\varrho = \pi r_f^2$ and $J = (2\pi r_f) \nu \Omega g_1 (1 + gm^2)$ on the right (outside the facet) to zero on the left.*

Intuitively, we view the zero values for ϱ and J as dictated by the totally collapsing step (with $R = 0$ for $\chi < \chi_f$) on top of the facet, where PDE (6.1) ceases to hold. We now show that Definition 6.1 can be made consistent with the subgradient formulation (section 5.1.1). By adopting the conventional theory of shocks, we choose to apply to the present setting the Rankine-Hugoniot condition [64], by which the shock speed is determined by conservation of volume across the jump. Thus, we write

$$(6.2) \quad \dot{\chi}_f(t) = -\dot{h}_f(t) = \frac{[J]}{[\varrho]},$$

where $[Q] = Q_{right} - Q_{left}$ is the discontinuity of $Q = \varrho, J$; see Appendix A.2. Equation (6.2) leads to (5.3).

6.2. Evaporation model as limit of BCF-type model. Next, we provide a modified evaporation-condensation model, M3, which is derived as a special limit of surface diffusion in the context of BCF theory [8, 50] in the presence of desorption and an inverse ES effect. M3 is subsequently simplified to another description, model M2, which has a structure resembling M1. Outside the facet, these models reduce to the same PDE for the slope profile. We provide numerical evidence that, for $g = 0$, discrete slopes produced by M2 are not in agreement with the subgradient-based continuum theory.

6.2.1. Formulation and simplifications. Let C_i be the concentration of adatoms on the i th terrace, $r_{i-1} < r < r_i$, and τ be a typical desorption time. In juxtaposition to our ad hoc model M1, here we adopt the viewpoint that the step velocity is driven by changes in the adatom flux across terraces. So, we start with a diffusion equation for the concentration, C_i , of adatoms including desorption under the quasi-steady approximation:

$$(6.3) \quad \frac{\partial^2 C_i}{\partial r^2} + \frac{1}{r} \frac{\partial C_i}{\partial r} - \kappa^2 C_i = 0, \quad r_{i-1} < r < r_i,$$

where $\kappa^2 = \frac{1}{D_s \tau}$. Equation (6.3) is Bessel's differential equation [63]; thus, it has the general solution

$$(6.4) \quad C_i(r) = A_i I_0(\kappa r) + B_i K_0(\kappa r),$$

where $I_0(z)$ and $K_0(z)$ are modified Bessel functions of zeroth order; and A_i and B_i are integration constants to be determined from the boundary conditions at the step edges. These conditions are

$$(6.5a) \quad -J_i(r, t) = D_s \frac{\partial C_i}{\partial r} = k_u (C_i - C_i^{\text{eq}}), \quad r = r_i,$$

$$(6.5b) \quad J_i(r, t) = -D_s \frac{\partial C_i}{\partial r} = k_d (C_i - C_{i+1}^{\text{eq}}), \quad r = r_{i+1},$$

where $J_i(r, t) = -D_s \frac{\partial C_i(r, t)}{\partial r}$ is the adatom flux on the i th terrace and C_i^{eq} is the equilibrium concentration at the i th step edge. By (6.4) and (6.5) we obtain

$$\begin{aligned} A_i &= \frac{1}{\mathcal{D}_i} \left\{ -\frac{k_u}{D_s k} C_i^{\text{eq}} \left[K_0'(\kappa r_{i+1}) + \frac{k_d}{D_s \kappa} K_0(\kappa r_{i+1}) \right] \right. \\ &\quad \left. - \frac{k_d}{D_s k} C_{i+1}^{\text{eq}} \left[K_0'(\kappa r_i) - \frac{k_u}{D_s \kappa} K_0(\kappa r_i) \right] \right\}, \\ B_i &= \frac{1}{\mathcal{D}_i} \left\{ \frac{k_d}{D_s \kappa} C_{i+1}^{\text{eq}} \left[I_0'(\kappa r_i) - \frac{k_u}{D_s \kappa} I_0(\kappa r_i) \right] \right. \\ &\quad \left. + \frac{k_u}{D_s \kappa} C_i^{\text{eq}} \left[I_0'(\kappa r_{i+1}) + \frac{k_d}{D_s \kappa} I_0(\kappa r_{i+1}) \right] \right\}, \end{aligned}$$

where the prime denotes differentiation with respect to the argument and

$$(6.6) \quad \begin{aligned} \mathcal{D}_i &= \left[I_0'(\kappa r_i) - \frac{k_u}{D_s \kappa} I_0(\kappa r_i) \right] \left[K_0'(\kappa r_{i+1}) + \frac{k_d}{D_s \kappa} K_0(\kappa r_{i+1}) \right] \\ &\quad - \left[I_0'(\kappa r_{i+1}) + \frac{k_d}{D_s \kappa} I_0(\kappa r_{i+1}) \right] \left[K_0'(\kappa r_i) - \frac{k_u}{D_s \kappa} K_0(\kappa r_i) \right]. \end{aligned}$$

The step velocity law for surface diffusion reads [8]

$$(6.7) \quad \dot{r}_i = \frac{\Omega}{a}(J_{i-1} - J_i), \quad r = r_i$$

By (6.4), the step velocity becomes

$$(6.8) \quad \dot{r}_i = -\frac{\Omega}{a}\kappa D_s [A_{i-1}I_0'(\kappa r_i) + B_{i-1}K_0'(\kappa r_i) - A_iI_0'(\kappa r_i) - B_iK_0'(\kappa r_i)].$$

We now simplify the expressions for A_i and B_i under the conditions

$$(6.9) \quad k_u\tau \ll r_i, \quad \kappa r_i \ll 1, \quad k_u \ll k_d, \quad |r_i - r_{i-1}| \ll k_d\tau.$$

Note that the second inequality implies that the diffusion length $\sqrt{D_s\tau}$ is large compared to the step radius. The third inequality expresses an inverse ES effect [15, 54].

By combining (6.8) and (6.9) with the Gibbs-Thomson relation [32], $C_i^{\text{eq}} = C^{\text{eq}}\exp(\mu_i/\mathcal{T}) \sim C^{\text{eq}}(1 + \mu_i/\mathcal{T})$ for $|\mu_i| \ll \mathcal{T}$, we obtain the simplified ODEs

$$(6.10) \quad \dot{r}_i = -\frac{\Omega}{\mathcal{T}a\tau} \frac{1}{2r_i} \frac{r_i + r_{i-1}}{2r_i} (r_i - r_{i-1})(\mathcal{T} + \mu_i),$$

where $\nu_i = \frac{r_i + r_{i-1}}{2r_i}(r_i - r_{i-1})$ is the step mobility. Equation (6.10) describes M3; cf. (1.2). Recall that model M2, equation (1.3), results from (6.10) by removal of the constant \mathcal{T} . Subsequently, M_1 results from replacing $(r_i + r_{i-1})/2r_i$ by 1 in the description of M2.

6.2.2. Numerical results on M2. We now provide numerical evidence that, for $g = 0$, the discrete slopes produced by ODEs (1.3) of M2 are not consistent with the continuum slope of the subgradient formulation. Note that the discrete mobility of M2 is $\nu\mathcal{G}(r_i - r_{i-1})$ and differs from the mobility of M1 by the prefactor $\mathcal{G} = \frac{r_i + r_{i-1}}{2r_i}$. Evidently, models M2 and M1 reduce to the same continuum theory in the macroscopic limit, since $\mathcal{G} \rightarrow 1$ in this limit.

From Figure 6.1, we observe that the positions of facets predicted by the two theories, i.e., ODEs for M2 and subgradient formulation, are different. This result contrasts our corresponding findings for M1; in particular, the facet size predicted by M2 is smaller than the one predicted by M1.

The discrepancy between models M1 and M2 is mainly attributed to the disparate behaviors of their mobilities near extremal steps. For model M1, the prefactor \mathcal{G} is 1 for all i . In M2, on the other hand, this factor becomes $\frac{1}{2}$ at the top step and then approaches 1 asymptotically as i increases.

The study of M3 lies beyond the scope of our work. An apparent feature of discrete slopes produced by this model (according to our numerics) is their lack of a self-similar structure. Hence, we do not deem as compelling a comparison of predictions of M3 to our results here.

7. Conclusion. We studied an example of a discrete scheme for a train of descending steps with a facet in the radial setting. The scheme expresses a simple mechanism of evaporation-condensation kinetics: steps move in response to the difference of the step chemical potential from that of the vapor. The relevant mobility is taken proportional to the width of the upper terrace. The resulting ODEs describe steps collapsing on top of the facet. On the other hand, the continuum limit expresses the height change with respect to time as the variational derivative of a familiar singular energy and can be analyzed via the (continuum) subgradient formulation. Our

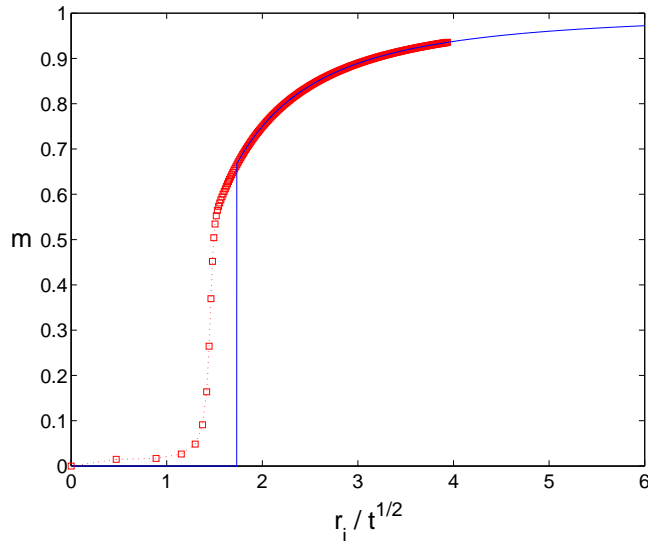


FIG. 6.1. Continuum slope $m(r, t)$ (solid line) and discrete slopes M_i (symbols) as functions of r/\sqrt{t} for long times, $g = 0$ and initial cone of unit slope. The slope $m(r, t)$ is computed from (5.19) and (5.21); and $M_i(t)$ are determined from numerically solving ODEs (1.3).

main finding via self-similarity of the slope, numerics and an initial conical shape is that the discrete slopes are in agreement with the slope profile predicted in the context of the subgradient theory.

The continuum limit of our model belongs to a class of widely used macroscopic theories for surface relaxation by evaporation [59]. Nonetheless, our primary discrete model (M1) was constructed from an ad hoc scenario of microscopic evaporation which essentially leaves out fine details and subtleties of the radial geometry; for instance, the mobility of M1 does not contain any geometric factor that distinguishes extremal from other steps. In fact, our model can stem from a simplification of a BCF-type model with desorption and an inverse ES effect. Our discussion suggests that the more realistic variants of M1 (herein called M2 and M3) that describe geometrically altered velocities of top steps may produce discrete slopes incompatible with the thermodynamics-based prediction. Our work suggests a mechanism, through the effect of the geometric factor \mathcal{G} (cf. (1.2)), that is plausibly responsible for the discrepancy between discrete and thermodynamics-based continuum solutions in the radial setting.

The proof of convergence of the discrete dynamics to the subgradient law was not touched upon. Loosely speaking, a difficulty in studying the connection of (discrete) step dynamics to continuum theories near facets lies in the lack of a method or prescription that defines the facet within the discrete system. In fact, the facet is typically viewed as a fully continuum concept. A goal is to understand if and how the notion of the facet can be defined in a discrete setting, asymptotically for a large number of steps. Motivated by this broader question, we proposed a shock wave interpretation of the facet which is compatible with the subgradient formulation (and, thus, with model M1 for a large number of steps). By use of Lagrangian coordinates, this interpretation qualitatively suggests that for our particular ad hoc model M1 the facet edge signifies a free boundary between two disparate behaviors: on the right of this boundary, step motion can be replaced by a PDE; on the left, the discrete

scheme reduces trivially to a collapsed step at the origin. It is a remarkable feature of model M1 that this simple continuum picture of Lagrangian coordinates is consistent (according to our numerics) with the step ODE solution.

In addition to our comparison of discrete and continuum dynamics, we proved the existence of a unique solution for the discrete system. (The existence of a unique solution for the continuum limit has been proven within the subgradient theory [22]). Also, we proved that steps do not collide when the initial step train is strictly monotone.

A few more remarks on open questions are in order. We stress that a proof of convergence to the continuum solution was not pursued here. Some technical complications stem from the nonlinear structure of step motion laws and influence of step collapses on top of the facet. The task of proving convergence is left for near-future work. The existence and nature of self-similar discrete and continuum solutions in our radial setting need to be addressed rigorously. Although our numerics indicate a self-similar structure of the slope, a precise description of the origin of this structure is still missing. The modified, closer to BCF-type theories, models M2 and M3 that we discussed briefly deserve more attention. Our study, so far limited to radial geometries with conical initial data, should be extended to the full 2D geometry. An ensuing difficulty is the possibility of meandering instabilities; to the best of our knowledge, there is no widely accepted measure of meandering for closed steps (say, perturbations of circles). For example, it is debatable whether our choice of implementing an inverse ES barrier results in an instability of a perturbed radial geometry; this issue is the subject of work in progress.

Appendix A. Elements of rigorous continuum theory.

In this appendix, we provide ingredients of known mathematical theories which have some relevance to the continuum description of facets. We focus on (i) the subgradient formalism, and (ii) the derivation of a formula, the conventional Rankine-Hugoniot condition for the shock speed, which is invoked in section 6.1. For ease of notation, vectors are *not* boldface in this appendix.

A.1. Concept of subgradient. We now briefly describe elements of the subgradient theory which underlies the free boundary approach of section 5.1.1, assuming some familiarity of the reader with functional analysis. The subgradient formalism provides a means of analyzing evolution laws that have a steepest descent structure with respect to a singular energy functional (i.e., the variable of interest evolves so that a non-smooth energy decreases most rapidly in some suitable metric [33, 47]). The singularities of the energy may correspond to points in space where the solution develops facets (plateaus) with moving boundaries. An elementary exposition to the subgradient system for a surface diffusion system can be found in [47].

Formally speaking, the notion of the subgradient extends the concept of conventional gradient (or derivative) to convex functions or functionals that are not necessarily differentiable everywhere. Let \mathcal{H} be a Hilbert space and F be a convex functional on \mathcal{H} . The subgradient, $\partial F(x)$, of F at the point x of \mathcal{H} is the set of all vectors v in \mathcal{H} that satisfy the inequality

$$(A.1) \quad F(x+h) - F(x) \geq \langle v, h \rangle \quad \text{for all } h \text{ in } \mathcal{H},$$

where $\langle v, h \rangle$ denotes the inner product of \mathcal{H} .

Consider first the classic example of the convex function $f(x) = |x|$ where $-1 \leq x \leq 1$. In this case, \mathcal{H} is the one-dimensional space $[-1, 1]$ equipped (trivially) with

the product of reals. Since $f(x)$ is differentiable at $x \neq 0$, we find $\partial f(x) = \{\text{sgn}(x)\}$, a singleton, where $\text{sgn}(x) = x/|x|$ is the sign function. The notion of $\partial f(x)$ becomes particularly useful for $x = 0$, where $f(x)$ is not differentiable. To compute $\partial f(0)$, one notices that for any real h , $f(h) - f(0) = |h| \geq |\varpi h|$ only if $|\varpi| \leq 1$. It is easily deduced that $\partial f(0) = [-1, 1]$, the set of all possible slopes of linear graphs bounded above by the graph of $y = |x|$ in the xy plane. This example can be extended to d space dimensions. Consider $f(x) = |x|$, where x is any point in the d -dimensional Euclidean space, \mathbb{R}^d . Then, $\partial f(x) = \{x/|x|\}$ if $x \neq 0$, and $\partial f(0) = B^d(0, 1)$.

The above ideas can be generalized to functionals, i.e., mappings of vectors in \mathcal{H} to real numbers, or more generally to its underlying algebraic field. A motivation for this generalization comes from the need to analyze evolution PDEs that have a steepest descent structure. An abstract formulation suggests that such evolutions can be viewed as ‘trajectories’ of elements of \mathcal{H} , in a way analogous to dynamical systems (ODEs). The associated evolution PDE for u is replaced globally by a statement of the form

$$(A.2) \quad \frac{du(t)}{dt} \in -\partial F(u(t)) \quad \text{for all } t > 0,$$

with the initial condition $u(0) = u_0 \in \mathcal{H}$. A known theorem of convex analysis asserts that there exists a unique (sufficiently smooth) $u(t)$ in \mathcal{H} for all $t > 0$ provided the functional F satisfies certain conditions such as appropriate convexity [22].

In particular, evolution PDE (4.7) for evaporation-condensation can be recast to form (A.2), where $u = h$ and $F(u) \equiv E(h) = \iint \gamma(\nabla h) dx$, the singular surface free energy (4.5); set $g_1 = 1$ and $g_3 = g$. The subgradient $\partial E(h)$ extends the variational derivative of $E(h)$ to the facet ($\nabla h = 0$) in a fashion analogous to the extension of the derivative of $f(x) = |x|$ to $x = 0$ through the notion of $\partial f(0)$. A characterization theorem for subgradient systems states that, for such a functional $F = E$, a function f belongs to $\partial F(h)$ if and only if there is a pair of continuous vector-valued functions ξ_1 and ξ_2 (in \mathbb{R}^2 for our purposes) satisfying [22]

$$(A.3) \quad f = \text{div}(\xi_1 + g\xi_2),$$

where ξ_1 is an element of $\partial J_1(\nabla h)$ and ξ_2 is an element of $\partial J_2(\nabla h)$ with $J_1(p) = |p|$ and $J_2(p) = |p|^3/3$. This characterization is a central ingredient of the formulation, with direct implications to boundary conditions at the facet. By virtue of formulas

$$(A.4) \quad \partial J_1(p) = \begin{cases} \{p/|p|\} & \text{if } p \neq 0 \\ B^2(0, 1) & \text{if } p = 0 \end{cases}, \quad \partial J_2(p) = \{|p|p\},$$

one can assert that $|\xi_1| \leq 1$ and $\xi_2 = 0$ for $p = 0$; therefore, $|\xi| \leq 1$ on the facet.

In conclusion, by (A.2)-(A.4), there exists a *continuous* vector-valued ξ such that

$$(A.5) \quad \partial_t h = -\text{div} \xi \quad \text{everywhere,}$$

where ξ belongs to $\partial \gamma(p)$ for $p = \nabla h$; in our radial setting, $|\xi| \leq 1$ for $r < r_f(t)$ and the term in ξ that multiplies g , i.e. the term corresponding to ξ_2 , is zero on the facet. This consideration leads to boundary conditions (5.3) and (5.5) for $g > 0$. Since m is continuous for $g > 0$, so is h . (For $g = 0$, this argument needs to be modified since m ceases to be continuous [33].)

A.2. Shock boundary condition. Next, we indicate a derivation of the conventional Rankine-Hugoniot condition for the shock speed, invoked in section 6.1, following the method in [16]. We apply the idea of an “integral solution” or “weak solution” of a PDE that has the form $\partial_t \varrho + \partial_\chi J = 0$ as does (6.1). By contrast to the case with steps of the main text, where the relevant PDE is defined *only on one side* of the shock (facet edge), our derivation here assumes that the PDE holds (in a weak sense) on both sides of the shock. This assumption results in the known Rankine-Hugoniot condition.

Consider a smooth, compactly supported test function $v(\chi, t)$ that is defined everywhere in the (χ, t) (spacetime) half-plane with $t \geq 0$. Also, define Γ to be the curve parameterized by $\chi = \chi_f(t)$, where jump discontinuities of the density ϱ and J may occur. In particular, choose v so that it is nonzero across Γ . Suppose that Γ is the common boundary of two regions: \mathcal{X}_r which corresponds to the region *right* of the shock (for $\chi > \chi_f$), and \mathcal{X}_l which corresponds to the region *left* of the shock. By multiplying the PDE $\partial_t \varrho + \partial_\chi J = 0$ by v and applying integration by parts (recalling that v vanishes for large enough χ and t) inside \mathcal{X}_r , we obtain

$$(A.6) \quad \begin{aligned} \iint_{\mathcal{X}_r} (\partial_t \varrho + \partial_\chi J) v \, dt d\chi &= - \iint_{\mathcal{X}_r} (\varrho \partial_t v + J \partial_\chi v) \, dt d\chi \\ &+ \int_{\Gamma} (\varrho_r n^t + J_r n^\chi) v \, ds, \end{aligned}$$

where $\hat{n} = (n^\chi, n^t)$ is the unit vector normal to Γ in the direction outward to \mathcal{X}_r ; and ϱ_r and J_r denote the limit values of ϱ and J on Γ from the right (the subscript r here should not be confused with the polar coordinate).⁷ Similarly, we compute the integral over \mathcal{X}_l :

$$(A.7) \quad \begin{aligned} \iint_{\mathcal{X}_l} (\partial_t \varrho + \partial_\chi J) v \, dt d\chi &= - \iint_{\mathcal{X}_l} (\varrho \partial_t v + J \partial_\chi v) \, dt d\chi \\ &+ \int_{\Gamma} (\varrho_l n^t + J_l n^\chi) v \, ds. \end{aligned}$$

By adding (A.6) and (A.7), we obtain

$$\int_{\Gamma} [(\varrho_r - \varrho_l) n^t + (J_r - J_l) n^\chi] v \, ds = 0.$$

Since this integral relation holds for all possible functions v , we conclude that

$$(A.8) \quad (\varrho_r - \varrho_l) n^t + (J_r - J_l) n^\chi = 0 \quad \text{on } \Gamma,$$

for all time $t \geq 0$. This condition leads to the conventional Rankine-Hugoniot condition, $\dot{\chi}_f(t) = [J]/[\varrho]$, via parameterizing \hat{n} in terms of $\chi_f(t)$.

Appendix B. On discrete equations with $g = 0$.

In this appendix, we solve exactly the equations of motion (2.12) with $g = 0$ for the two top steps, aiming to obtain a recursion relation for the time differences $\delta_n = t_n - t_{n-1}$. Our results enable us to check the accuracy of our numerical scheme for solving the step ODEs. We employ units with $\nu \Omega g_1 = 1 = a$.

⁷More precisely, ρ_r and J_r denote the traces of ρ and J on Γ from the right.

First, consider times $t_{n-1} < t < t_n$ for fixed collapse number n ($n \geq 1$). For $g = 0$, (2.12) reduce to

$$(B.1) \quad \dot{r}_i = -\frac{r_i - r_{i-1}}{r_i} \quad i \geq n.$$

In particular, for $i = n$ we have $\dot{r}_n = -1$ by which

$$(B.2) \quad r_n(t) = t_n - t, \quad t_{n-1} < t \leq t_n.$$

We proceed to determine $r_{n+1}(t)$, which satisfies $r_{n+1}\dot{r}_{n+1} = -r_{n+1} + t_n - t$ in view of (B.2). We seek a solution in parametric form by using another independent variable, say, τ . Let $t_n - t \equiv \sigma(\tau)$ and $r_{n+1}(t) \equiv \sigma(\tau)p(\tau)$ where σ and p are to be determined. The ODE for $r_{n+1}(t)$ yields

$$(B.3) \quad \frac{\dot{\sigma}}{\sigma} = -\frac{\dot{p}p}{p^2 - p + 1},$$

which can be integrated exactly; $\dot{\sigma} \equiv d\sigma/d\tau$. By setting $p(\tau) = \tau$ (without loss of generality), we find $\sigma(\tau)$ and thereby compute t and r_{n+1} as functions of τ :

$$(B.4) \quad \begin{aligned} r_{n+1}(t(\tau)) &= C(\tau^2 - \tau + 1)^{-1/2} \tau e^{\mathcal{K}(\tau)}, \\ t(\tau) &= t_n - C(\tau^2 - \tau + 1)^{-1/2} e^{\mathcal{K}(\tau)}, \end{aligned}$$

where $\tau > \tau_*$ (and τ_* depends on n) and

$$(B.5) \quad \mathcal{K}(\tau) = \frac{1}{2\sqrt{3}} \tan^{-1} \left[\frac{\sqrt{3}(1 - 2\tau)}{1 + 2\tau - 2\tau^2} \right].$$

The (in principle n -dependent) constants C and τ_* are determined by the initial conditions $t(\tau_*) = t_{n-1}$ and $r_{n+1}(t(\tau_*)) = r_{n+1}(t_{n-1}) \equiv \mathfrak{R}_n$. Thus, we obtain

$$(B.6) \quad \begin{aligned} t(\tau) &= t_n - \delta_n \left(\frac{\tau_*^2 - \tau_* + 1}{\tau^2 - \tau + 1} \right)^{1/2} e^{\mathcal{K}(\tau) - \mathcal{K}(\tau_*)}, \\ r_{n+1}(t(\tau)) &= \delta_n \left(\frac{\tau_*^2 - \tau_* + 1}{\tau^2 - \tau + 1} \right)^{1/2} \tau e^{\mathcal{K}(\tau) - \mathcal{K}(\tau_*)}, \end{aligned}$$

where

$$(B.7) \quad \tau_* = \frac{\mathfrak{R}_n}{\delta_n}.$$

As the n th step collapses, $t \uparrow t_n$ and thus $\tau \rightarrow \infty$; the radius $r_{n+1}(t_n)$ follows from (B.6).

Now consider times $t_n < t < t_{n+1}$, after the n th step collapses. Then, $r_{n+1}(t) = t_{n+1} - t$. By continuity of $r_{n+1}(t)$ and use of (B.6), we find the recursion relation

$$(B.8) \quad \frac{\delta_{n+1}}{\delta_n} = \sqrt{\tau_{*,n}^2 - \tau_{*,n} + 1} e^{-\mathcal{K}(\tau_{*,n})},$$

where $\tau_{*,n} \equiv \tau_* = \mathfrak{R}_n/\delta_n = r_{n+1}(t_{n-1})/\delta_n$.

It is of interest to discuss implications of (B.8) in the limit $n \rightarrow \infty$, under the assumption that $\delta_{n+1}/\delta_n \gtrsim 1$. By (B.8), $\tau_{*,n}$ cannot approach 0. If in addition δ_{n+1}/δ_n is assumed to be bounded with n , as is presumably the case for an initial conical profile (where $r_i(0)$ is linear in i), we assert that $\tau_{*,n}$ must approach a finite value: $\tau_{*,n} \rightarrow \tau_o$ as $n \rightarrow \infty$. Thus, τ_o obeys

$$(B.9) \quad (\tau_o^2 - \tau_o + 1)^{1/2} e^{-\mathcal{K}(\tau_o)} = 1.$$

By numerically solving this transcendental equation, we find $\tau_o \approx 1.66$, in agreement with our (independent) numerical simulations for (2.12).

Appendix C. On near-facet expansion for $m(\eta)$.

In this appendix, we provide the coefficients c_l for the sum S_k introduced in (5.27) with $k = 13$. In this vein, we also invoke the coefficients, d_l , of expansion $\mathcal{M}_1(s) \sim \sum_{l=1}^k d_l s^l$. By dominant balance in the similarity ODE (5.23) along with the facet condition (5.24) and after some algebra we derive the following formulas.

$$\begin{aligned} d_0 &= c_0 = 0, & d_1 &= (\eta_f g)^{-1}, & c_1 &= \sqrt{d_1}, & d_2 &= -c_1 \eta_f / (3g), & c_2 &= d_2 / (2c_1), \\ d_3 &= -\frac{\eta_f c_2}{4g} + \frac{1}{2g\eta_f^2} + \frac{c_1^2}{2\eta_f}, & c_3 &= \frac{d_3 - c_2^2}{2c_1}, & d_4 &= -\frac{4}{15\eta_f^2} \left(\frac{3\eta_f^2 c_1 + 3\eta_f^3 c_3}{4g} + 3d_2 \eta_f \right), \\ c_4 &= \frac{d_4 - 2c_2 c_3}{2c_1}, & d_5 &= -\frac{1}{6\eta_f^2} \left(\frac{3c_2 \eta_f^2 + 2c_4 \eta_f^3}{2g} + 6d_3 \eta_f \right), & c_5 &= \frac{d_5 - 2c_2 c_4 - c_3^2}{2c_1}, \\ d_6 &= -\frac{4}{35\eta_f^2} \left(\frac{3c_1 \eta_f + 9c_3 \eta_f^2 + 5c_5 \eta_f^3}{4g} + 5d_2 / 4 + 10d_4 \eta_f \right), & c_6 &= \frac{d_6 - 2c_2 c_5 - 2c_3 c_4}{2c_1}, \\ d_7 &= -\frac{1}{12\eta_f^2} \left(\frac{3c_2 \eta_f + 6c_4 \eta_f^2 + 3c_6 \eta_f^3}{2g} + 3d_3 + 15d_5 \eta_f \right), & c_7 &= \frac{d_7 - 2c_2 c_6 - 2c_3 c_5 - c_4^2}{2c_1}, \\ d_8 &= -\frac{4}{63\eta_f^2} \left(\frac{c_1 + 9c_3 \eta_f + 15c_5 \eta_f^2 + 7c_7 \eta_f^3}{4g} + 21d_4 / 4 + 21d_6 \eta_f \right), \\ c_8 &= (d_8 - 2c_2 c_7 - 2c_3 c_6 - 2c_4 c_5) / (2c_1), \\ d_9 &= -\frac{1}{20\eta_f^2} \left(\frac{c_2 + 6c_4 \eta_f + 9c_6 \eta_f^2 + 4c_8 \eta_f^3}{2g} + 8d_5 + 28d_7 \eta_f \right), \\ c_9 &= (d_9 - 2c_2 c_8 - 2c_3 c_7 - 2c_4 c_6 - c_5^2) / (2c_1), \\ d_{10} &= -\frac{4}{99\eta_f^2} \left(\frac{3c_3 + 15c_5 \eta_f + 21c_7 \eta_f^2 + 9c_9 \eta_f^3}{4g} + 45d_6 / 4 + 36d_8 \eta_f \right), \\ c_{10} &= (d_{10} - 2c_2 c_9 - 2c_3 c_8 - 2c_4 c_7 - 2c_5 c_6) / (2c_1), \\ d_{11} &= -\frac{1}{30\eta_f^2} \left(\frac{2c_4 + 9c_6 \eta_f + 12c_8 \eta_f^2 + 5c_{10} \eta_f^3}{2g} + 15d_7 + 45d_9 \eta_f \right), \\ c_{11} &= (d_{11} - 2c_2 c_{10} - 2c_3 c_9 - 2c_4 c_8 - 2c_5 c_7 - c_6^2) / (2c_1), \\ d_{12} &= -\frac{4}{143\eta_f^2} \left(\frac{5c_5 + 21c_7 \eta_f + 27c_9 \eta_f^2 + 11c_{11} \eta_f^3}{4g} + 77d_8 / 4 + 55d_{10} \eta_f \right), \\ c_{12} &= (d_{12} - 2c_2 c_{11} - 2c_3 c_{10} - 2c_4 c_9 - 2c_5 c_8 - 2c_6 c_7) / (2c_1), \\ d_{13} &= -\frac{1}{42\eta_f^2} \left(\frac{3c_6 + 12c_8 \eta_f + 15c_{10} \eta_f^2 + 6c_{12} \eta_f^3}{2g} + 24d_9 + 66d_{11} \eta_f \right), \\ c_{13} &= (d_{13} - 2c_2 c_{12} - 2c_3 c_{11} - 2c_4 c_{10} - 2c_5 c_9 - 2c_6 c_8 - c_7^2) / (2c_1). \end{aligned}$$

Acknowledgments. The authors wish to thank Professors Robert V. Kohn, Ricardo Nochetto, Olivier Pierre-Louis, and Ray Phaneuf as well as the late Professor John Osborn for stimulating discussions. The first author (K. Nakamura) is grateful to the University of Maryland for a Graduate Student Summer Research Fellowship during the summer of 2011.

REFERENCES

- [1] H. AL HAJJ SHEHADEH, *The Evolution of a Crystal Surface: Step ODEs, PDEs and Self-similarity*, Ph.D. thesis, Courant Institute, New York University, New York, NY, 2010.
- [2] H. AL HAJJ SHEHADEH, R. V. KOHN, AND J. WEARE, *The evolution of a crystal surface: Analysis of a one-dimensional step train connecting two facets in the ADL regime*, *Physica D*, 240 (2011), pp. 1771–1784.
- [3] S. BARTELS, *Total variation minimization with finite elements: Convergence and iterative solution*, preprint.
- [4] G. BIRKHOFF AND S. MACLANE, *A Survey of Modern Algebra*, MacMillan, New York, 1959.
- [5] L. BOLTZMANN, *Lectures on Gas Theory*, Dover, New York, 1995.
- [6] H. P. BONZEL, *3D equilibrium crystal shapes in the new light of STM and AFM*, *Phys. Rep.*, 385 (2003), pp. 1–67.
- [7] H. P. BONZEL, E. PREUSS, AND B. STEFFEN, *The dynamical behavior of periodic surface profiles on metals under the influence of anisotropic surface-energy*, *Appl. Phys. A-Mater.*, 35 (1984), pp. 1–8.
- [8] W. K. BURTON, N. CABRERA, AND F. C. FRANK, *The growth of crystals and the equilibrium structure of their surfaces*, *Philos. Trans. R. Soc. London Ser. A*, 243 (1951), pp. 299–358.
- [9] N. CABRERA AND D. A. VERMILYEA, *The Growth of Crystals from Solution*, in *Growth and Perfection of Crystals*, R. H. Doremus, B. W. Roberts, and D. Turnbull, eds., Wiley, New York, 1958, pp. 393–410.
- [10] A. CHAME, S. ROUSSET, H. P. BONZEL, AND J. VILLAIN, *Slow dynamics of stepped surfaces*, *Bulgarian Chem. Commun.*, 29 (1996/97), pp. 398–434.
- [11] A. CHAMBOLE AND T. POCK, *A first-order primal-dual algorithm for convex problems with applications to imaging*, *J. Math. Imaging Vis.*, 40 (2011), pp. 120–145.
- [12] E. A. CODDINGTON AND N. LEVINSON, *Theory of Ordinary Differential Equations*, McGraw-Hill, Boston, MA, 1955, pp. 13–15.
- [13] R. M. CORLESS, G. H. GONNET, D. E. G. HARE, D. J. JEFFREY, AND D. E. KNUTH, *On the Lambert W function*, *Adv. Comput. Math.*, 5 (1996), pp. 329–359.
- [14] W. E AND N. K. YIP, *Continuum theory of epitaxial growth. I*, *J. Stat. Phys.*, 104 (2001), pp. 221–253.
- [15] G. EHRLICH AND F. HUDDA, *Atomic view of surface diffusion: Tungsten on tungsten*, *J. Chem. Phys.*, 44 (1966), pp. 1039–1099.
- [16] L. C. EVANS, *Partial Differential Equations*, American Mathematical Society, Providence, RI, 1998.
- [17] P.-W. FOK, *Simulation of Axisymmetric Stepped Surfaces with a Facet*, Ph.D. thesis, Massachusetts Institute of Technology, Cambridge, MA, 2006.
- [18] P.-W. FOK, R. R. ROSALES, AND D. MARGETIS, *Unification of step bunching phenomena on vicinal surfaces*, *Phys. Rev. B*, 76 (2007), 033408.
- [19] P.-W. FOK, R. R. ROSALES, AND D. MARGETIS, *Facet evolution on supported nanostructures: Effect of finite height*, *Phys. Rev. B*, 78 (2008), 235401.
- [20] F. C. FRANK, *On the Kinematic Theory of Crystal Growth and Dissolution Processes*, in *Growth and Perfection of Crystals*, R. H. Doremus, B. W. Roberts, and D. Turnbull, eds., Wiley, New York, 1958, pp. 411–419.
- [21] M.-H. GIGA AND Y. GIGA, *Very singular diffusion equations: second and fourth order problems*, *Japan. J. Ind. Appl. Math.*, 27 (2010), pp. 323–345.
- [22] M.-H. GIGA, Y. GIGA, AND R. KOBAYASHI, *Very singular diffusion equations*, *Adv. Stud. Pure Math.*, 31 (2001), pp. 93–126.
- [23] L. GRÁNÁSY, T. BÖRZSŃYI, AND T. PUSZTAI, *Nucleation and bulk crystallization in binary phase field theory*, *Phys. Rev. Lett.*, 88 (2002), 206105.
- [24] E. E. GRUBER AND W. W. MULLINS, *On the theory of anisotropy of crystalline surface tension*, *J. Phys. Chem. Solids*, 28 (1967), pp. 875–887.
- [25] J. K. HALE, *Ordinary Differential Equations*, Willy-Interscience, Providence, RI, 1969, pp. 12–22.

- [26] C. HERRING, *Effect of change of scale on sintering phenomena*, J. Appl. Phys., 21 (1950), pp. 301–303.
- [27] C. HERRING, *Some theories on the free energies of crystal surfaces*, Phys. Rev., 82 (1951), pp. 87–93.
- [28] M. H. HOLMES, *Introduction to Perturbation Methods*, Springer, New York, 1998.
- [29] B. R. HUNT, R. L. LIPSMAN, J. E. OSBORN, AND J. ROSENBERG, *Differential Equations with Matlab*, Wiley, New York, 2005.
- [30] N. ISRAELI AND D. KANDEL, *Profile of a decaying crystalline cone*, Phys. Rev. B, 60 (1999), pp. 5946–5962.
- [31] N. ISRAELI AND D. KANDEL, *Decay of one-dimensional surface modulations*, Phys. Rev. B, 62 (2000), pp. 13707–13717.
- [32] H.-C. JEONG AND E. D. WILLIAMS, *Steps on surfaces: Experiments and theory*, Surf. Sci. Rep., 34 (1999), pp. 171–294.
- [33] R. KOBAYASHI AND Y. GIGA, *Equations with singular diffusivity*, J. Stat. Phys., 95 (1999), pp. 1187–1220.
- [34] R. V. KOHN, T. S. LO, AND N. K. YIP, *Continuum Limit of a Step Flow Model of Epitaxial Growth*, in Statistical Mechanical Modeling in Materials Science, MRS Symposia Proceedings 701, M. C. Bartelt, J. W. Evans, A. S. Karma, S. Torquato, and D. E. Wolf, eds., Materials Research Society, Warrendale, PA, 2002, pp. T1.7.1–T1.7.7.
- [35] J. KRUG, *On the shape of wedding cakes*, J. Stat. Phys., 87 (1997), pp. 505–518.
- [36] A. E. LOBKOVSKY AND J. A. WARREN, *Sharp interface limit of a phase-field model of crystal grains*, Phys. Rev. E, 63 (2001), 051605.
- [37] V. I. MARCHENKO AND A. YA. PARSHIN, *Elastic properties of crystal surfaces*, Sov. Phys. JETP, 52 (1980), pp. 129–131.
- [38] D. MARGETIS, M. J. AZIZ, AND H. A. STONE, *Continuum approach to self-similarity and scaling in morphological relaxation of a crystal with a facet*, Phys. Rev. B, 71 (2005), 165432.
- [39] D. MARGETIS, P.-W. FOK, M. J. AZIZ, AND H. A. STONE, *Continuum theory of nanostructure decay via a microscale condition*, Phys. Rev. Lett., 97 (2006), 096102.
- [40] D. MARGETIS AND R. V. KOHN, *Continuum relaxation of interacting steps on crystal surfaces in 2+1 dimensions*, Multiscale Model. Simul., 5 (2006), pp. 729–758.
- [41] D. MARGETIS AND K. NAKAMURA, *From crystal steps to continuum laws: Behavior near large facets in one dimension*, Physica D, 240 (2011), pp. 1100–1110.
- [42] T. MICHELY AND J. KRUG, *Islands, Mounds and Processes in Crystal Growth Far From Equilibrium*, Springer, Berlin, 2004.
- [43] C. MISBAH, O. PIERRE-LOUIS, AND Y. SAITO, *Crystal surfaces in and out of equilibrium: A modern view*, Rev. Mod. Phys., 82 (2010), pp. 981–1040.
- [44] W. W. MULLINS, *The effect of thermal grooving on grain boundary motion*, Acta Metall., 6 (1958), pp. 414–427.
- [45] R. NAJAFABADI AND J. R. SROLOVITZ, *Elastic step interactions on vicinal surfaces of fcc metals*, Surf. Sci., 317 (1994), pp. 221–234.
- [46] P. NOZIÈRES, *On the motion of steps on a vicinal surface*, J. Phys. (France), 48 (1987), pp. 1605–1608.
- [47] I. V. ODISHARIA, *Simulation and analysis of the relaxation of a crystalline surface*, Ph.D. thesis, Courant Institute, New York University, New York, NY, 2006.
- [48] M. OZDEMIR AND A. ZANGWILL, *Morphological equilibration of a corrugated crystalline surface*, Phys. Rev. B, 42 (1990), pp. 5013–5024.
- [49] A. PIMPINELLI, V. TONCHEV, A. VIDECOQ, AND M. VLADIMIROVA, *Scaling and universality of self-organized patterns on unstable vicinal surfaces*, Phys. Rev. Lett., 88 (2002), 206103.
- [50] A. PIMPINELLI AND J. VILLAIN, *Physics of Crystal Growth*, Cambridge University Press, Cambridge, UK, 1998.
- [51] A. RAMASUBRAMANIAM AND V. B. SHENOY, *On the evolution of faceted grain-boundary grooves by surface diffusion*, Acta Mater., 53 (2005), pp. 2943–2956.
- [52] A. RETTORI AND J. VILLAIN, *Flattening of grooves on a crystal surface: A method of investigation of surface roughness*, J. Phys. (France), 49 (1988), pp. 257–267.
- [53] M. SATO, *Effect of step permeability on step instabilities due to alternation of kinetic coefficients on a growing vicinal face*, Eur. Phys. J. B, 59 (2007), pp. 311–318.
- [54] R. L. SCHWOEBEL AND E. J. SHIPSEY, *Step motion on crystal surfaces*, J. Appl. Phys., 37 (1966), pp. 3682–3686.
- [55] W. SELKE AND P.M. DUXBURY, *Equilibration of crystal surfaces*, Phys. Rev. B, 52 (1995), pp. 17468–17479.
- [56] V. B. SHENOY AND L. B. FREUND, *A continuum description of the energetics and evolution of stepped surfaces in strained nanostructures*, J. Mech. Phys. Solids, 50 (2002), pp. 1817–

- 1841.
- [57] F. SLANINA, J. KRUG, AND M. KOTRLA, *Kinetics of step bunching during growth: A minimal model*, Phys. Rev. E, 71 (2005), 041605.
 - [58] H. SPOHN, *Large Scale Dynamics of Interacting Particles*, Springer, Berlin, 1991.
 - [59] H. SPOHN, *Surface dynamics below the roughening transition*, J. Phys. I (France), 3 (1993), pp. 69–81.
 - [60] H. A. STONE, M. J. AZIZ, AND D. MARGETIS, *Grooving of a grain boundary by evaporation-condensation below the roughening transition*, J. Appl. Phys., 97 (2005), 113535.
 - [61] M. UWABA, *Relaxation of crystal shapes caused by step motion*, J. Phys. Soc. Jpn., 57 (1988), pp. 1681–1686.
 - [62] M. UWABA AND K. WATANABE, *Decay of an island on a facet via surface diffusion*, J. Phys. Soc. Jpn., 69 (2000), pp. 497–503.
 - [63] G. N. WATSON, *A Treatise on the Theory of Bessel Functions*, Cambridge University Press, 2nd Ed., Cambridge, UK, 1995, pp. 77–78.
 - [64] G. B. WHITHAM, *Linear and Nonlinear Waves*, Wiley, New York, 1974.